POD-BASED FLOW ESTIMATION AND ITS APPLICATION IN CONTROL OF UNDERWATER ROBOTS

by

Fengying Dang

A Thesis
Submitted to the
Graduate Faculty
of
George Mason University
In Partial fulfillment of
The Requirements for the Degree
of
Master of Science
Electrical Engineering

Committee:

_____	Dr. Feitian Zhang, Thesis Director
_____	Dr. Cameron Nowzari, Committee Member
_____	Dr. Daniel M Lofaro, Committee Member
_____	Dr. Monson H Hayes, Department Chair
_____	Dr. Kenneth Ball, Dean, Volgenau School of Engineering

Date: _____ Fall Semester 2018
George Mason University
Fairfax, VA

POD-based Flow Estimation and Its Application in Control of Underwater Robots

A thesis submitted in partial fulfillment of the requirements for the degree of Master of Science at George Mason University

By

Fengying Dang
Bachelor of Science
Northwestern Polytechnic University, 2015

Director: Dr. Feitian Zhang, Assistant Professor
Department of Electrical and Computer Engineering

Fall Semester 2018
George Mason University
Fairfax, VA

Dedication

To My Family: mom, dad and my younger brother

Acknowledgments

I want to thank my father and mother who support me so many years and give me so much love. My father taught me the importance of being strong and a meaningful person for the world. I learned from my mother to be kind and nice. I also would like to thank my brother for his continues support and love. You are the greatest family one can ask for. During my study Dr. Cameron Nowzari and Dr. Daniel M Lofaro also give me a lot of support. Last but not least, I would like to thank my advisor, Dr. Feitian Zhang, without you all these things won't happen. Thank you all for your unconditional love and support, it has been, without a doubt, a key factor to my success.

Table of Contents

List of Tables

List of Figures

Abstract

POD-BASED FLOW ESTIMATION AND ITS APPLICATION
IN CONTROL OF UNDERWATER ROBOTS

Fengying Dang

George Mason University, 2018

Thesis Director: Dr. Feitian Zhang

Flow estimation plays an important role in the control and navigation of autonomous underwater robots. It is challenging for underwater robots because of the complex and dynamic fluid environment. Scientists and engineers have been making great efforts in improving flow estimation capability of underwater robots over the past years. There are two main methods to sense the flow field: (1) using flow sensors to measure flow fields directly; and (2) assimilating other sensor measurements (e.g, pressure) through flow estimation algorithms to estimate the flow field. Since the existing flow measurement equipment, such as pitometer log, is hulking, research about using on board sensors to do the flow estimation has attracted more and more attention. However, most of these algorithms can only be used for a specified shape of underwater vehicle.

This thesis presents a novel flow estimation approach that assimilates distributed pressure measurements through coalescing recursive Bayesian estimation and flow model reduction using proper orthogonal decomposition (POD). The proposed flow estimation approach does not rely on any analytical flow model and is thus applicable to many and various complicated flow fields for arbitrarily shaped underwater robots while most of the existing flow estimation methods apply only to well-structured flow fields with simple robot geometry.

This thesis also analyzes and discusses the flow estimation design in terms of reduced-order model accuracy, relationship with conventional flow parameters, and distributed senor placement. To demonstrate the effectiveness of the proposed distributed flow estimation approach, two simulation studies, one with a circular-shaped robot and one with a Joukowski-foil-shaped robot, are presented. The application of flow estimation in closed-loop angle-of-attack regulation is also investigated through simulation.

Chapter 1: Introduction

1.1 Motivation and Background

1.1.1 Motivation

Autonomous underwater robots attract increasing scientific attentions for their agile, long-range operation and great human-labor efficiency [1–5]. Their scope of application crosses various fields including environmental monitoring, search and rescue, surveillance and security, scientific research and public education. In recent years, underwater robotics has achieved many advances in terms of locomotion efficiency [2, 5], actuation mechanism [3], battery power endurance [4] etc., however, there is still one unsolved fundamental research problem—the flow estimation, which plays an essential role for control and navigation of autonomous underwater robots.

1.1.2 Background

Oceans attract a lot of attention from researchers because it covers 71% area of our earth. We need to explore our ocean for many reasons, such as resources and knowledge of the biology. People began to explore the ocean since many years ago, but it is dangerous for human beings to do so. Thus underwater robots are created by engineers to explore the underwater with reliability and safety. The traditional underwater vehicles are Remotely Operated Vehicle (ROV) and Autonomous Underwater Vehicle (AUV). But they both have some disadvantages such as system complexity, huge volume, low mobility and high price. All these disadvantages impulse the development of new underwater robots. The underwater creatures live underwater for a long time and have many good characteristics such as high efficiency, low noise, agility and high mobility. The bio-inspired underwater robots which

borrow ideas form nature creature may have better performance and have attracted more and more attentions from researchers. [6].

Since fish are the most common creatures in oceans, robotic fish became the most common bio-inspired underwater robot. Many different bio-inspired robots have been made, such as Robo Tuna [7], AmphiRobot [8], carangiform swimming robot [9], Robotic dolphin [10], Sea bream [11, 12], G9 robotic fish [13, 14], a dolphin-like underwater robot [15], a submersible vehicle based on sea turtles [16], ostraciiform modes underwater robot called BoxyBot [17], Nanyang Arowana-like fish (NAF) employing a carangiform swimming mode [18], a small low-cost teleoperated underwater robotic fish [19], AmphiRobot-II with multimode motion [20], Ray-like Fish Robots [21].

Model Identification of underwater vehicle

Getting an accurate and complete model of underwater vehicles is important and difficult for an underwater vehicle [22–24]. In 1987, Ljung used discrete-time method to identify the parameters of underwater vehicles [25]. But discrete-time method sometimes can be error prone. In 1998, Alessandri used least square algorithm and extended Kalman Filter to identify the model while neglected the cable effect. They concluded that identifying the parameters of small underwater vehicles is realizable. They also claimed that this method was low cost since it only uses standard on board device [26]. The Kalman filtering technique was also used to estimate the vehicle model to help with dynamic positioning of ships as described in [27] and [28]. In 2004, Ridao used a nonlinear continuous time method to identify the parameters of underwater vehicles. The advantages of using continuous time model is that the system will have global validity and through it we can get a variety of discrete-time models to be applied to the design of control fault detection system. They used both the direct Least Square(LS) method and the integral Least Square(LS) method which are two different kinds of off-line methods to identify the parameters of non-linear models in this thesis [29]. In 2005, the neural networks method was used to identify the parameters of underwater vehicles. This method is an online learning method which can

identify parameters of nonlinear system[30]. In 2006, Tiano used observer Kalman filter algorithm to identify parameters of a linear discrete-time multi-variable model. Also both the linear and nonlinear yaw dynamic have been tested using observer Kalman identification(OKID)[31]. Several researchers have reported their results using extended Kalman filter which treats the parameters as additional state variables. In [32], an extended Kalman Filter (EKF) has been used to estimate the model for maneuver trials of Esso Osaka both in deep and shallow water. In [33], EKF and the model reference approaches are used for system identification to maneuver trials of a surface ship. The extended Kalman Filter are also used in [34, 35]and [36]. Further work based on the extended Kalman filter in the field of system identification is accomplished by [37] and [38].

Identification of flow field

Underwater vehicle works in the complex and dynamic environments, so it is very important for them to sense the flow field around them.

Estimating a flow field requires a mathematical flow model that is typically obtainable through one of the many methods such as analytical flow modeling [39–41], computational fluid dynamics (CFD) simulation [42] and towing tank experiments [43]. The analytical flow modeling method is easy-to-implement and cost-effective. However, this method is only suitable to special-shaped robots. For example, [39], [40] [41] take Joukowski foil as the shape of underwater robots and use potential flow model for flow estimation, thus limiting this flow sensing method to those robots with the same foil shape described by a conformal mapping function. CFD simulation on the other hand can provide accurate flow models for underwater robots with any designed shape. However, even with a simplified CFD model such as the panel method used in [42], the flow model still cannot be used in real-time flow estimation due to the high computational cost. Towing tank experiments are commonly used in a well-controlled lab environments. With the help of flow visualization methods such as particle image velocimetry [43], the flow model can be experimentally established. However, it is not suitable for autonomous underwater robots that typically

operate in open water.

Flow estimation is a challenging problem for underwater robots because of the complex flow environment. Some existing research seeks to establish the relationship between flow parameters and flow measurements as analytical functions [44,45]. Some others develop flow sensing algorithms to estimate the flow based on commonly used sensors, such as pressure sensors [2,40,41,46]. Considering the complexity of the flow field, the estimators commonly used include a Kalman estimator [40] and a Bayesian filter [2, 41, 46]. In [47], Lagor used a Bayesian filter to estimate fish orientation and free-stream flow speed based on potential flow model. In [39], the author used measurements from multi-modal artificial lateral line to estimate the uniform flow around fish robot. Based on potential flow theory, they use a nonlinear estimation strategies to estimate free stream flow speed, angel of attack and relative position of an upstream obstacle. Although effective in estimating specific flow fields, most of the existing flow sensing algorithms are limited to simple flow fields and special robot designs.

Some research used a distributed sensor network sensor information form different vehicle. It has a promising future to characterize some of the environmental phenomena [48].

Actuators of Underwater Robot

The traditional actuators are wildly used on underwater robots to propel the underwater robot, e.g., motors, joints, links and so on. In [7], a segmented backbone with low friction ball bearing joints are used as the actuators of Robo Tuna. In [8], links, passive wheels and synchromesh belt are used in the propulsive mechanism. In [9], servomotor was used to power the fish system. In [10], three links and six servomotors were used in propulsive mechanism of Robotic dolphin. In [11] and [12], joints, servomotors and linear bearings were used in the design of fish robot. In [13], 3 servo motors were used to drive the fish. In [15], gear wheels, motor, rack and pinion were used to construct the tail mechanism. In [16], a combination of a stepping motor, a crank mechanism and a universal joint were used for forefins which represent flapping motion. In [17], joints are used to provide degree

of freedom to pectoral and caudal fin. In [18], some joint and pins were used as the actuators of the fish robot. In [19], motors are used to propel the robotic fish. In [20], wheel propeller-fin, modular fishlike propelling units and composite peduncle were used in the propulsive mechanic system of robotic fish. In [21], six servo motors were used to drive the fin rays of the robot and let it swim.

Recently years with the development of material science, more and more new actuator are used on underwater robot. These smart actuators have the ability to perform flexible and complex movement with high efficiency. Their aim is to make the robot smaller and lighter. Shape memory alloys (SMAs) [49–53], ionic polymer-metal composite (IPMCs) [54–56], artificial muscle [57], and lead zirconate titanate (PZT) [58] are the popular smart actuator. Also some combined actuator were also used bu some researchers [59, 60].

In summary, the common used actuators on bio-inspired robots are

1. Servo motor
2. Piezoelectric Ceramics
3. Shape memory alloy
4. Artificial muscles
5. combined actuator

Future Development of Bio-inspired Underwater Robot

The traditional underwater vehicles can dive deeply into the sea with its thick shell; bio-inspired robotics is the robots imitating the pattern, movements and functions of the underwater creatures, such as the fish-inspired robots, lobster-inspired robots and worm-inspired robots referred before. Bio-inspired robotics can move flexibly and have a high energy utilization. There are some aspects we can do to improve the performance of bio-inspired underwater vehicles.

1. The improvement of actuated device

   Traditional actuated device is driven by motor, but as the development of new material, such as memory alloy, piezoelectric ceramics and artificial muscles, many different kinds of new actuators will substitute the traditional devices to decrease the heavy and volume of the actuator.

2. Movement mechanism improvement of bio-inspired underwater robots

   As the research on the underwater creatures going deeply and deeply, we will know more about the movement mechanism of bio-inspired underwater robots and increase the swimming efficiency.

3. Intelligence improvement of underwater vehicles

   Now most of the bio-inspired underwater robots are in the semi-intelligent condition, as the development of artificial science, automatic control, computer technology, the bio-inspired underwater robots will have more intelligent abilities, e.g., interacting with the environment, protecting themselves under harsh condition, working in complex conditions and so on.

4. Working in a group

   The group of fish will performance better when escape the enemy and catch small fish. The single underwater vehicle will have a limit area and moving ability. But underwater vehicles are expected to work in a complex environment in the future, so group underwater vehicles which can cooperate with each other and have a high efficiency is the trend in developing underwater vehicles.

1.2 State of Art and Limitations

1.2.1 Related Work

Flow estimation is challenging because the underwater environment is complex and thus has limited the navigation and control ability of underwater vehicle.

Various types of flow sensors have been designed to estimate the flow field directly. Ships use acoustic instruments such as acoustic Doppler current profilers (ADCP) to measure water velocity. However, ADCPs are expensive and have a dead zone in proximity to the underwater vehicle [61, 62]. Based on thermal principles, [63, 64] designed a micromachined hot-wire flow sensor. This sensor was tested in a manually varied laminar flow to show the ability of detecting flow rate. In [65], a flow sensor based on torque transfer was presented where a static turbine converted the volume flow into a torque measurement. Optical flow sensors were used to obtain hydrodynamic information in [66, 67]. In [66], the authors used optical flow sensors to measure the flow motion inside artificial canals and then quantified the pressure gradient. In [67], an optical feedback interferometry flow sensor was designed and used to measure the local flow velocity. A crystal polymer MEMS sensor was designed for flow estimation in [68, 69]. This sensor was able to detect the velocity of towed underwater objects [68] and flow speed and direction [69]. Recently more and more flow sensors have been developed, which have high spatial resolution and short response time. However, these designs are mostly customized and ad hoc solutions with a long design cycle and relatively high cost. These disadvantages impede broad real-world applications in autonomous underwater robots.

Parallel to designing flow sensors to directly measure local flow velocity, more and more research efforts have been put into using multiple low-cost, commercially available sensors and a flow estimation algorithm to estimate the whole flow field. Inspired by the high performance of fish lateral line, scientists and engineers have been making great efforts in developing similar flow-sensing systems [39, 40, 42, 43, 45, 46, 70, 71]. The lateral line helps aquatic vertebrates sense surrounding flow fields and assists with flow relative behaviors, such as rheotaxis, predation and schooling [72]. Some papers use linear regression to approximate the flow field [45], while others use nonlinear estimation algorithms including Extended Kalman Filter(EKF) [40], Bayesian Filter [39, 46, 70, 71], Unscented Kalman Filter(UKF) [42], Particle Filter [43], to assimilate distributed (pressure and velocity) sensor measurements for flow sensing.

In [70], author used a recursive Bayesian filter to estimate the theoretical flow field parameters which are used to steer the vehicle to a desired orientation through simulation. The flow estimation method was verified using experiments in [39]. In [39], a recursive Bayesian filtering algorithm is used to estimate a parameterized uniform flow-field using ionic polymer metal composite and embedded pressure sensors. In [73], Bayesian estimation is used on a soft robotic fish to estimate a quasi steady potential flow based on multiple pressure sensor outputs. In [71], author used a Bayesian filter estimation methods on a flexible fish robot and test a closed-loop control strategy with the estimated flow as feedback. An extended Kalman filter based on pressure information is used to estimate the hydrodynamic coefficients in [40]. In [74], an ensemble Kalman filter(FEM) is used to estimate a shallow water flow field based on water elevation. In our prior work [46, 71], co-author Zhang studied flow estimation for a Joukowski hydrofoil locomoting in a uniform flow using a Bayesian filter. In [46], the same flow estimation method as [71] was used to do flow-relative-speed and turning-rate control in two-dimensional free swimming with a flexible fish robot actuated by a reaction wheel. The flow estimation based on Bayesian filter has been demonstrated excellent flow estimation ability.

The flow estimation algorithms typically require a mathematical flow model, which is obtainable through one of the many methods such as analytical flow modeling [39,40,46,70, 71], computational fluid dynamics (CFD) simulation [42] and towing tank experiments [43, 45]. The analytical flow modeling method is easy-to-implement and cost-effective. However, this approach is only suitable to special-shaped robots. For example, the potential flow model in [39] and [46] can only be used with the same foil shape described by a conformal mapping function. CFD simulation on the other hand can provide accurate flow models for underwater robots with any designed shape. However, even with a simplified CFD model such as the panel method used in [42], the flow model still cannot be used in real-time flow estimation due to the computational cost. Towing tank experiments are commonly used in a well-controlled lab environments. With the help of flow visualization methods such as particle image velocimetry [43], the flow model can be experimentally established. However,

it is not suitable for autonomous underwater robots that typically operate in open water.

1.2.2 Limitations

Existing flow measurement equipment, such as pitometer log, is used to measure the relative speed between the vehicle and water. But these kind of equipment is bulk and low measurement accuracy. Some micromachined flow sensors based on a few principles, such as doppler shifts [61], frequency thermal anemometry [63, 64] and torque transfer [65], were designed during past years. These sensors are mostly customized and ad hoc solutions with a long design cycle and relatively high cost. These disadvantages impede broad real-world applications in autonomous underwater robots.

The flow estimation based on Bayesian filter has been demonstrated excellent flow estimation ability. Although estimation performances were satisfactory, our prior designs, like most existing flow sensing algorithms have very serious limitation that they only apply to specific flow fields. To solve this problem, a novel flow estimation algorithm that coalesces recursive Bayesian estimation and flow model reduction using proper orthogonal decomposition (POD) has been put forward in this thesis. This algorithm supposes to broaden the use of flow estimation algorithm based on Bayesian dramatically.

1.3 Proposed Work

This thesis proposes a general flow estimation approach using distributed pressure measurements of autonomous underwater robots via integrating proper orthogonal decomposition (POD)-based flow models and recursive Bayesian estimation. Proper orthogonal decomposition is a data-driven model reduction method that is often used to analyze fluid fields. It was first introduced by Lumley [75] in 1979 and has been widely used since then. This approach can be applied to arbitrary robot designs and reduce the computational cost. At the same time, this thesis adopts a Bayesian filter to assimilate the distributed pressure measurements for flow estimation. The likelihood calculation of the Bayesian estimator is integrated with a reduced-order POD flow model.

The contribution of this thesis lies in (1) a novel real-time flow estimation algorithm that assimilates distributed pressure measurements by integrating recursive Bayesian estimation and POD-based reduced-order flow modeling; and (2) quantitative analysis of flow model reduction accuracy and sensor placement through proposing performance metrics utilizing POD modeling percent error and empirical observability analysis, respectively. There are three main advantages of the proposed method. First, POD-based flow modeling reduces the computational complexity thus making real-time flow estimation possible. Second, the POD-based flow estimation using a Bayesian filter does not rely on any analytical flow models, thus applicable to any underwater robot with arbitrary shape designs. Third, our flow estimation method is based on low-cost commercially available pressure sensors, thus especially useful in small and networked autonomous underwater robots.

The remainder of the thesis is organized as follows. Section 2 presents the POD flow model reduction algorithm and the Bayesian filter approach that estimates the flow field by assimilating distributed pressure measurements. Section 3 discusses the POD flow model reduction accuracy, relationship between the POD model and conventional flow parameters of interest, and sensor placement strategy. In Section 4, two simulation examples illustrate the proposed flow estimation method with a cylinder shaped robot and a Joukowski-foil-shaped robot. In Section 5, the closed-loop angle-of-attack regulation is investigated in simulation which utilizes the proposed flow estimation algorithm. Finally, conclusion remarks are presented in Section 6.

Chapter 2: Distributed Flow Estimation

In this section, we present a general flow estimation approach that assimilates distributed pressure measurements of autonomous underwater robots via integrating POD reduced-order flow models and recursive Bayesian estimation.

2.1 POD-based Flow Model Reduction

Proper orthogonal decomposition or POD is a model reduction method, which decomposes a nonlinear and high-dimensional or infinite-dimensional system into a lower dimensional system using finite number of basis POD modes based on a large set of data. The optimal set of POD modes to represent the system are determined based on L_2 norm optimization using the POD algorithm [75].

In fluid dynamics, potential flow is used to describe the velocity field as the gradient of a scalar function— the velocity potential [76]. As a result, a potential flow is characterized by an irrotational velocity field. In the case of an incompressible flow the velocity potential satisfies Laplace's equation, and potential theory is applicable.

In this thesis, the POD algorithm deals with flow field snapshots that represent the velocity or pressure field, obtained from either CFD simulation, theoretical calculation or towing tank experiments. Optimal POD modes and corresponding coefficients are calculated and used to model the flow field. The procedure of POD calculation is as follows.

First, obtain M flow field snapshots $\boldsymbol{U}_1, \boldsymbol{U}_2, \ldots, \boldsymbol{U}_M$, each of which is generated under certain values of flow parameters of interest, such as the flow speed and the angle of attack. Every snapshot includes i rows and j columns of points that represent the local flow velocity. Each snapshot is described by an $a \times b$ dimensional matrix.

Second, reshape each flow field snapshot matrix into a column vector. Use vector $\boldsymbol{u}_i$ to describe the flow field snapshot $\boldsymbol{U}_i$. Concatenating all the column vectors into a new matrix, we get the flow field snapshot matrix $\boldsymbol{U} = [\boldsymbol{u}_1, \boldsymbol{u}_2, \cdots, \boldsymbol{u}_M]$ whose dimension is $a \times b$ by M.

Then we calculate the correlation matrix [75, 77]

$$\boldsymbol{R} = \boldsymbol{U} \times \boldsymbol{U}^{\boldsymbol{T}} \tag{2.1}$$

Through eigenvalue decomposition we can get the eigenvalues of the correlation matrix $\boldsymbol{R}$, sorted in the descending order, $\lambda = \{\lambda_1, \lambda_2, \ldots, \lambda_q\}$ and their corresponding eigenvectors $\boldsymbol{v} = \{\boldsymbol{v}_1, \boldsymbol{v}_2, \ldots, \boldsymbol{v}_q\}$, where q is the rank of matrix $\boldsymbol{R}$ [75]. The corresponding POD coefficients for flow field snapshot i are $c_{i1}, c_{i2}, \ldots, c_{iq}$, given by

$$c_{ij} = \langle \boldsymbol{u}_i, \boldsymbol{v}_j \rangle \qquad j \in \{1, 2, \cdots, q\} \tag{2.2}$$

where the POD coefficients are calculated by the inner product of the flow field vector $\boldsymbol{u}_i$ and the POD mode vector $\boldsymbol{v}_j$.

Reconstruction of the flow field is then given by [75, 77]

$$\hat{\boldsymbol{U}}_i = \sum_{j=1}^{O} c_{ij} \boldsymbol{v}_j \qquad i \in \{1, 2, \cdots, M\} \tag{2.3}$$

where O, less than q, is the selected number of POD modes in the reduced-order flow model, and $\hat{\boldsymbol{U}}_i$ represents the reconstructed ith flow field snapshot in a vector form.

2.2 Distributed Flow Estimation via Integration of a Bayesian Filter and POD Flow Model Reduction

With the flow field modeled by the reduced-order POD model, we use a Bayesian filter to assimilate distributed pressure measurements and estimate the coefficients of POD modes. This section presents our distributed flow estimation method that coalesces a Bayesian filter and POD flow model reduction.

Define the sensor position vector as $\boldsymbol{z} = [z_1, z_2, \ldots, z_N]^{\mathrm{T}} \in \mathbb{C}^N$ with positional elements ordered in a counter clockwise direction along the underwater robot body. If we use p_i to represent the theoretical flow pressure at sensor position z_i, then the pressure vector is given by $\boldsymbol{p} = [p_1, p_2, \ldots, p_N]^{\mathrm{T}} \in \mathbb{R}^N$. According to Bernoulli's equation, the pressure distribution along the streamline around the underwater robot is [78],

$$p_i = C - \frac{1}{2}\rho\frac{\partial(F(z_i) + \overline{F(z_i)})}{\partial t} - \frac{1}{2}\rho|w(z_i)|^2 \tag{2.4}$$

where C is a constant, F is the complex potential of the flow field, w is the local flow velocity and ρ is the flow density.

We assume the pressure measurements are corrupted with Gaussian noise ε_i, i.e.,

$$\tilde{p}_i = p_i + \varepsilon_i \tag{2.5}$$

where $\tilde{p}_i$ is the actual pressure sensor measurement at sensor position z_i, and ε_i is Gaussian with a mean of zero and a variance of σ_i^2, i.e., $\varepsilon_i \sim (0, \sigma_i^2)$.

Inspired from the lateral line of fish, we use pressure difference between sensor pair as the flow measurement function [72], i.e., $\triangle\tilde{p}_{ij}(t) = \tilde{p}_i(t) - \tilde{p}_j(t)$. In this thesis, we assume flow fields change slowly compared to the fast sampling from pressure sensors. Thus we ignore the unsteady effect in flow estimation and the flow measurement function becomes $\triangle\tilde{p}_{ij} = \tilde{p}_i(t) - \tilde{p}_j(t) = \frac{1}{2}\rho|w(z_j)|^2 - \frac{1}{2}\rho|w(z_i)|^2$.

We use $\triangle\tilde{\boldsymbol{p}}_{ij}(t)$ to represent the time series of pressure difference measurements between

sensors i and j until time t, defined as

$$\triangle\tilde{\boldsymbol{p}}_{ij}(t) = [\triangle\tilde{p}_{ij}(t), \triangle\tilde{p}_{ij}(t-\triangle t), \ldots, \triangle\tilde{p}_{ij}(0)]^{\mathrm{T}} \quad i \neq j \tag{2.6}$$

All the flow measurement data up to time t is defined as $\boldsymbol{D}(t)$, i.e.,

$$\boldsymbol{D}(t) = [\triangle\tilde{\boldsymbol{p}}_{12}(t), \triangle\tilde{\boldsymbol{p}}_{13}(t), \cdots, \triangle\tilde{\boldsymbol{p}}_{(N-1)N}(t)] \tag{2.7}$$

Here, we use all the pairs of pressure difference between all the sensors rather than mimicking the lateral line that uses only pressure difference between adjacent sensors. Using all possible pairs will help reduce the estimation error considering the averaging effect over more noisy measurements, thus improving estimation accuracy.

We define the flow measurement vector at time t as $\boldsymbol{D_c}$, i.e.,

$$\boldsymbol{D_c} = [\triangle\tilde{p}_{12}, \triangle\tilde{p}_{13}, \cdots, \triangle\tilde{p}_{(N-2)(N-1)}, \triangle\tilde{p}_{(N-1)N}]^{\mathrm{T}} \tag{2.8}$$

A Bayesian filter is adopted to estimate the POD coefficients' probability density function recursively using the incoming pressure measurements. In this thesis, O normalized POD modes $\boldsymbol{v}_1, \boldsymbol{v}_2, \ldots, \boldsymbol{v}_O$ are chosen for the flow field, and the corresponding POD coefficients at time t are denoted by $\wedge = [c_1, c_2, c_3, \ldots, c_O]^T$, defined as the estimation state of the Bayesian filter. The POD reduced-order flow model is then given by

$$\boldsymbol{u_c} = \sum_{j=1}^{O} c_k \boldsymbol{v}_k \qquad k \in \{1, 2, \cdots, O\} \tag{2.9}$$

The update of the probability density function follows Bayes' rule, i.e.,

$$Pr(\wedge|\boldsymbol{D}(t)) = \kappa Pr(\boldsymbol{D_c}|\wedge) Pr(\wedge|\boldsymbol{D}(t-\triangle t)) \tag{2.10}$$

where κ is the coefficient that ensures the probability of the entire sample space equals 1,

$Pr(\boldsymbol{D_c}|\wedge)$ is the likelihood function of new measurement $\boldsymbol{D_c}$ given the coefficients of the POD modes $\wedge$, $Pr(\wedge|\boldsymbol{D}(t))$ is the posterior probability density function, and $Pr(\wedge|\boldsymbol{D}(t-\triangle t))$ is the prior probability density function.

Assuming the pressure sensor measurement is corrupted with Gaussian noise, we have a Gaussian likelihood function, i.e.,

$$Pr(\boldsymbol{D_c}|\wedge) = \frac{1}{\sqrt{2\pi}\sigma_i} \exp(\frac{-(\boldsymbol{D_s} - \boldsymbol{D_c})^2}{2\sigma_i^2}) \tag{2.11}$$

where $\boldsymbol{D_s} = [\triangle p_{12}, \triangle p_{13}, \ldots, \triangle p_{(N-2)N-2}, \triangle p_{(N-1)N}]^T$ represents the theoretical values of the flow measurements calculated using the POD flow model (2.9).

The prior pdf is predicted using the Chapmon-Kolmogorov equation [79], i.e.,

$$\begin{aligned} Pr(\wedge(t)|\boldsymbol{D}(t-\triangle t)) = \int Pr(\wedge(t)|\wedge(t-\triangle t))\times \\ Pr(\wedge(t-\triangle t)|\boldsymbol{D}(t-\triangle t))\mathrm{d}\wedge(t-\triangle t) \end{aligned} \tag{2.12}$$

where $Pr(\wedge(t)|\wedge(t-\triangle t))$ represents a general motion model, the solution of which typically requires solving ordinary/partial differential equations with advection/diffusion.

The process of the distributed flow estimation method for underwater robots is summarized as follows. First, we obtain the optimal reduced-order POD modes that models the flow field around the underwater robot from the snapshots of the flow field. When the robot receives new sensor measurements, the likelihood function $Pr(\boldsymbol{D_c}|\wedge)$ is computed using the reduced-order flow model. Given a prior probability density function $Pr(\wedge(t)|\boldsymbol{D}(t-\triangle t))$, the posterior probability density function is updated based on the Bayes' rule (2.10). Through the posterior probability density function $Pr(\wedge(t)|\boldsymbol{D}(t))$ we determine the current optimal POD coefficients $\wedge$, selected as the point in the estimation state space with the highest joint posterior pdf. The Chapmon-Kolmogorov equation predicts the prior pdf $Pr(\wedge(t)|\boldsymbol{D}(t-\triangle t))$ at time t based on the posterior pdf $Pr(\wedge(t-\triangle t)|\boldsymbol{D}(t-\triangle t))$

at time $t - \triangle t$.

This thesis uses a POD reduced-order flow model to compute the likelihood function $Pr(\boldsymbol{D_c}|\wedge)$ and estimates the flow parameters $\wedge$ through distributed pressure measurements $\boldsymbol{D_c}$. The adoption of the reduced-order flow model is expected to significantly improve the computational efficiency and the application scope.

2.3 Flow Sensing Algorithm Summary and Its Advantages

The process of our proposed flow sensing algorithm is summarized as in Figure 2.1. First we get the POD modes through snapshots we get in experiments or simulation. When the fish swim in the water, we estimate the POD coefficients for the POD modes using Bayesian filter based on sensor output. We get the estimated flow model using the POD modes and estimated POD coefficients.

The most important advantage of the proposed flow sensing algorithm is they can be widely used on different shapes of robotic fish. The adoption of the POD-based flow reduction model in the recursive Bayesian filter largely increase the range of the use of this flow estimation. The reason is that POD flow model is a mode based flow model and thus won't constrained this algorithm to a certain shape of underwater robot. Also, this algorithm is based on the pressure sensor which is usually a on board sensor. Existing flow measurement equipment, such as pitometer log, is used to measure the relative speed between the vehicle and water. However, they are bulk and sometimes low measurement accuracy. These disadvantages of existing flow measurement equipment let this algorithm with the normal pressure sensors have a promising future.

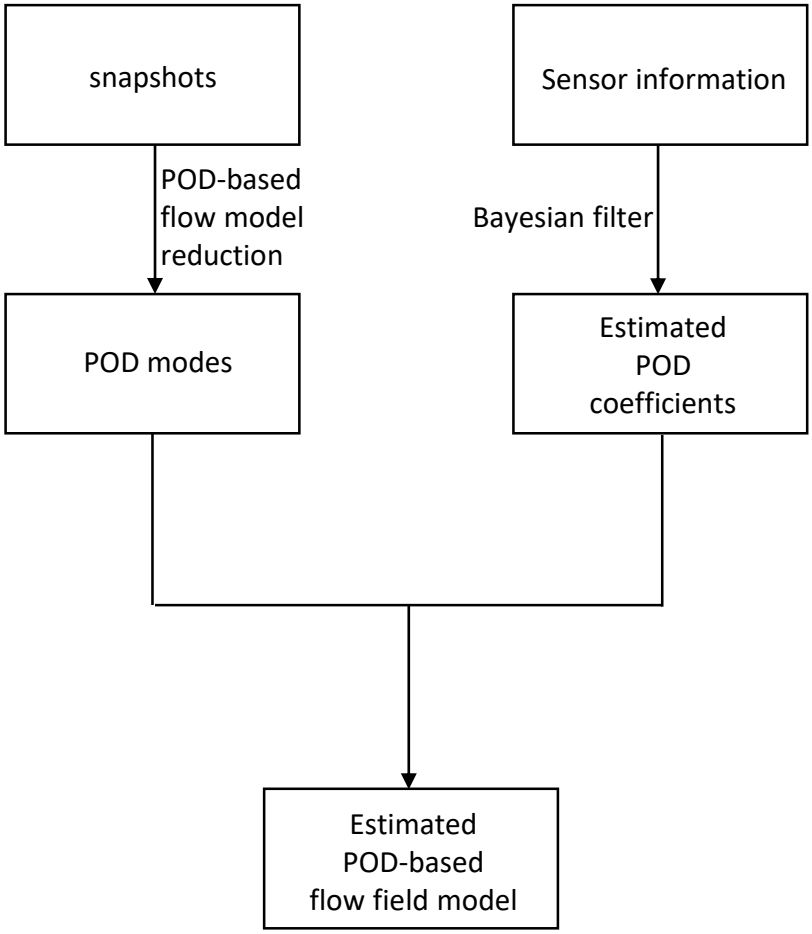

Figure 2.1: Flow chart of the proposed POD-based flow sensing that assimilates distributed pressure measurements through coalescing recursive Bayesian estimation and flow model reduction using proper orthogonal decomposition (POD).

Chapter 3: Flow Estimation Design Analysis

In this section, we analyze the proposed flow estimation approach, in terms of the accuracy of the POD flow model reduction, the mapping between POD coefficients and conventional flow parameters, and the sensor placement strategy.

Performance index are proposed for studying model reduction and sensor placement. The proposed performance index depend on many design factors such as number of pressure measurements, the size of the snapshot, flow conditions, etc. The focus of this section is to provide a general approach for researching model reduction design and sensor placement strategy with quantified measures, therefore, we have chosen to minimize the discussions on the influences of different factors. Interested readers are encouraged to refer to sensitivity analysis [80] and use tools therefrom to explore the influences of different designs.

3.1 POD Reduced-Order Modeling Accuracy

The reduced-order modeling accuracy of a flow field has a strong relationship with the selected number of POD modes. For example, Fig. 3.1 shows the modeling error with different number of POD modes in a simulation case study of modeling the flow field of a Joukowski-foil-shaped robot in a uniform flow. From the simulation results, we can see that using one POD mode leads to a large modeling error in a considerable area of the flow field. With two or more POD modes, the area with a large modeling error reduces dramatically, resulting in a more accurate constructed flow field. The drawback is that more number of POD modes leads to more computational cost. To address the balance between modeling accuracy and computational cost, this thesis proposes a performance index $\bar{E}$, the POD modeling percent error to assist with the POD mode selection, defined as

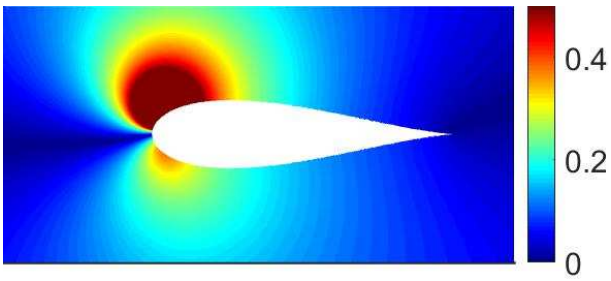

(a) one mode

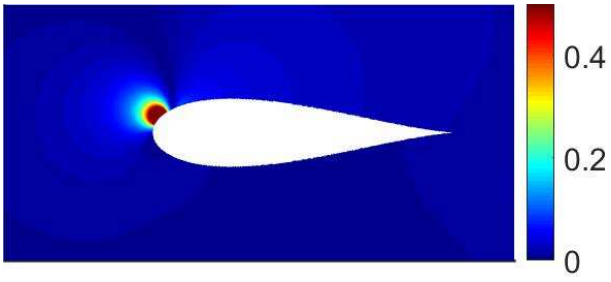

(b) two modes

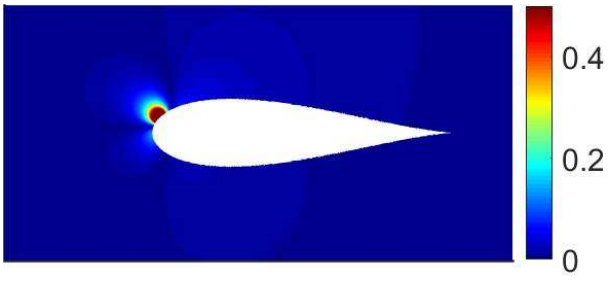

(c) three modes

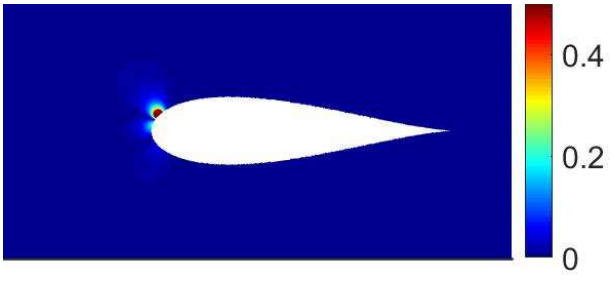

(d) four modes

Figure 3.1: The simulation results of the reduced-order modeling error for the flow field around a Joukowski-foil-shaped robot using different numbers of POD modes. The color map represents the distribution of the velocity difference between the actual flow field and the reconstructed flow field using POD model reduction.

$$\bar{E} = \frac{\sum_i \sum_j |\frac{\hat{\boldsymbol{U}}(i,j) - \boldsymbol{U}(i,j)}{\boldsymbol{U}(i,j)}|}{i \times j} \tag{3.1}$$

where $\hat{\boldsymbol{U}}$ is the reconstructed flow field snapshot matrix using POD model reduction, $\boldsymbol{U}$ is the flow field snapshot matrix. $\bar{E}$ represents the averaged modeling percent error given a certain number of POD modes.

Table 3.1: The POD modeling percent error given different numbers of POD modes for the simulation results in Figure 3.1.

Number of POD modes	POD modeling percent error $\bar{E}$
One	2.57%
Two	0.18%
Three	0.16%
Four	0.07%

Table 3.1 shows the POD modeling percent error $\bar{E}$ given different numbers of POD modes for the same uniform flow past a Joukowski-foil-shaped robot used in the case study as in Fig. 3.1. The modeling percent error $\bar{E}$ is about 2.57% with one POD mode and reduces to 0.18% with two POD modes. The proposed performance index $\bar{E}$ quantifies the reduced-order modeling error and clearly shows that more POD modes lead to higher modeling accuracy. Considering the balance between computational cost and model reduction accuracy, a minimum number of POD modes will be selected to meet the flow estimation design requirements.

3.2 Mapping Between the POD Coefficients and Conventional Flow Parameters

Some conventional flow parameters, for example, the flow speed and the angle of attack, are very important variables in determining/estimating the hydrodynamics and control/navigation of autonomous underwater robots. However, most of the flow parameters like the angle of attack are very difficult if not impossible to measure with on-board sensors as they require the flow field information. Therefore, once we are able to estimate the flow field described by the POD reduced-order model (Section 2), we proceed to extract or calculate the relevant flow parameters using the estimated flow field.

Considering the nonlinear and complex relationship between the flow parameters like the angle of attack and estimated flow field parameterized by POD coefficients, we propose to use the neural network technique to establish the mapping. Neural network is a computing system that is usually organized in layers and can approximate nonlinear systems based on sampled training data [81–83]. Neural networks, composed of parallel-working nodes, imitates the biological neural system. The most common structure of a neural network includes an input layer, single/multiple hidden layer(s) and an output layer as shown in Fig. 3.2. The input and output layers of the neural network in our application are decided by the number of POD modes and flow parameters. The original flow field snapshots and the corresponding calculated POD mode coefficients are used to train the neural network.

In this section, we will introduce how to use neural network to find the mapping between the angle of attack and the estimated POD flow model, in particular, the POD mode coefficients. In this thesis, the Matlab Neural Network Toolbox is used to train the network. We are going to compare the mapping accuracy using different neural network settings. The development of a neural network including the following steps as shown in Fig. 3.3. The details of each step is described in details below.

1. Get the training data

   We use simulation to get some snapshots of the velocity around the robotic fish. Some

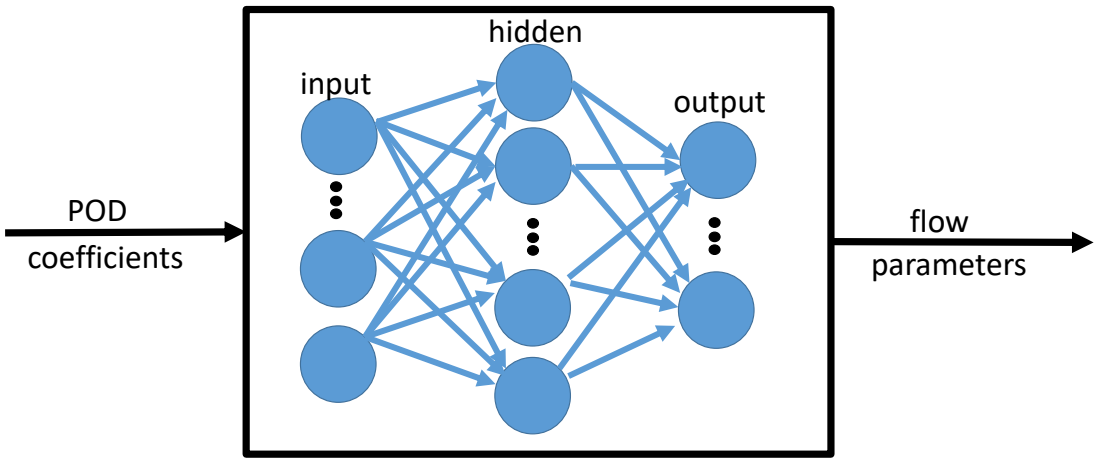

Figure 3.2: The neural network structure to approximate the relationship between flow parameters and the POD coefficients.

of these snapshots are taken as training data in the neural network, while others are taken as the validating data.

2. Create the neural network

   Design a neural network structure you want use to approximate the relationship between flow parameters and the POD coefficients. Mainly the number of layers and nodes in the hidden layer.

3. Configure the network's inputs and outputs

   Decide the number of inputs and outputs based on your own problem. Here we want to find the mapping between the angle of attack and the estimated POD flow model, in particular, the POD mode coefficients. For example, if we choose two POD modes, then there will be two inputs (two POD coefficients) and one output (angle of attack).

4. Tune the network parameters (the weights and biases) to optimize performance

   Find the optimal weights and biases for the designed neural.

5. Train the network

6. Validate the network's results

   Using validating data to validate the trained neural network.

7. Integrate the network into a production system

3.3 Sensor Placement Strategy

Sensor placement affects the flow field estimation because different sensor positions contain different volume of flow field information. We propose to optimize sensor placement using the concept of system observability [70,84]. While the observability is difficult to capture or theoretically compute, we will leverage the empirical observability Gramian to quantify the observability of the estimation states or the POD coefficients and design a sensor placement strategy thereby.

The empirical observability Gramian[70, 84] of our flow estimation system is calculated as

$$\boldsymbol{W_O} = \frac{1}{4\varepsilon_i\varepsilon_j}\langle \triangle p_{\text{sum}}^{+i} - \triangle p_{\text{sum}}^{-i}, \triangle p_{\text{sum}}^{+j} - \triangle p_{\text{sum}}^{-j} \rangle$$

$$i = 1, \ldots, O, j = 1, \ldots, O \tag{3.2}$$

Here, $\triangle p_{\text{sum}} = |\triangle \tilde{p}_{12}| + |\triangle \tilde{p}_{13}| + \cdots + |\triangle \tilde{p}_{(N-1)N}|$ is the sum of absolute value of all the pairwise pressure differences with pressure sensor positioned at certain locations given the POD coefficients $\wedge = [c_1, c_2, c_3, \ldots, c_O]^T$. ε_i is a small perturbation of the ith POD coefficient, $\triangle p_{\text{sum}}^{+i}$ is the sum of absolute value of all the pairwise pressure differences when the POD coefficients are equal to $\wedge = [c_1, \ldots, c_i + \varepsilon_i, \ldots, c_O]^T$, $\langle x, y \rangle$ denotes the inner product of complex numbers x and y [39].

Since the leading POD modes capture the majority of flow field information, the first two POD coefficients c_1 and c_2 are selected to evaluate the observability with respect to

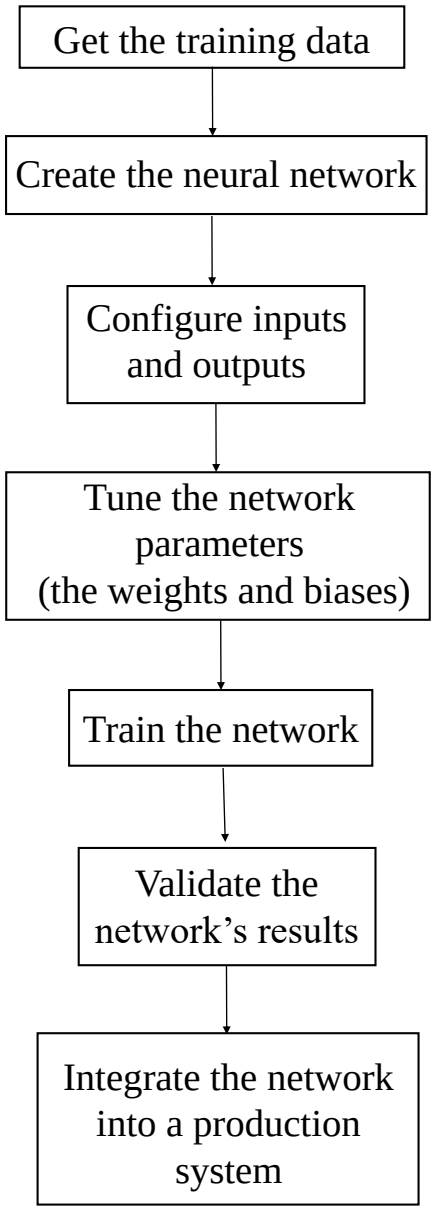

Figure 3.3: The workflow of developing a neural network to approximate the relationship between flow parameters and the POD coefficients.

different sensor positions. The empirical observability Gramian is then given by

$$\boldsymbol{W}_O = \begin{bmatrix} \frac{\delta p_{c_1} \delta p_{c_1}}{\triangle c_1 \triangle c_1} & \frac{\delta p_{c_1} \delta p_{c_2}}{\triangle c_1 \triangle c_2} \\ \frac{\delta p_{c_1} \delta p_{c_2}}{\triangle c_1 \triangle c_2} & \frac{\delta p_{c_2} \delta p_{c_2}}{\triangle c_2 \triangle c_2} \end{bmatrix} \tag{3.3}$$

where δp_{c_i} is the change of $\triangle p_{\text{sum}}$ when the ith POD mode coefficient has a perturbation $\pm\varepsilon_i$ about c_i, and, $\triangle c_i = (c_i + \varepsilon_i) - (c_i - \varepsilon_i) = 2\varepsilon_i$ is the overall perturbation of the ith POD mode coefficient.

From the empirical observability Gramian, we compute characteristic index (I_1, I_2, I_3) as follows.

The first index I_1 represents the unobservability of flow parameter c_1, defined as a function of $\boldsymbol{W}_O(1,1)$ which corresponds to a perturbation in the first POD coefficient.

$$I_1 = \log(\boldsymbol{W}_O(1,1)^{-1}) \tag{3.4}$$

Similarly, the second index I_2, describing the unobservability of the POD coefficient c_2, is defined as

$$I_2 = \log(\boldsymbol{W}_O(2,2)^{-1}) \tag{3.5}$$

The third index I_3, representing the error covariance, is defined as the log of the inverse trace of the empirical unobservability matrix, i.e.,

$$I_3 = \log(\text{trace}(\boldsymbol{W}_O)^{-1}) \tag{3.6}$$

An an example, Fig. 3.4 shows the simulation results of the three indices evaluated at different sensor positions that are represented by polar angles in the same case study with a Joukowski-foil-shaped robot as in Fig. 3.1. We consider four sensors for flow estimation, located symmetrically on two sides of the robots. We also consider the dimension of the

sensors and define a minimal separation distance to avoid sensor overlapping. Here the simulation results are based on flow speed at 0.3 m/s and angle of attack at 0° which are considered to be one of the nominal working point in the robot state space. The optimal sensor placement for observing POD coefficient c_1 is one sensor near the polar angle 160.21° and the second sensor near 159.39°, while the optimal sensor placement for observing c_2 is one sensor near 168.15° and the second sensor near 153.42°. The selection of sensor positions near the polar angle 169.04° and 168.15° minimizes index I_3.

Based on the observability indices, we propose the following composite performance index to assist with the sensor placement,

$$I_c = l_1 I_1 + l_2 I_2 + l_3 I_3 \tag{3.7}$$

where l_1, l_2, and l_3 are the design coefficients that balance the weights of performance indices. In sensor placement design, we will use simulation/experiment to search for optimal sensor positions that minimize the composite index to achieve maximum observability. The proposed strategy facilitates the design process through providing a convenient quantitative metric.

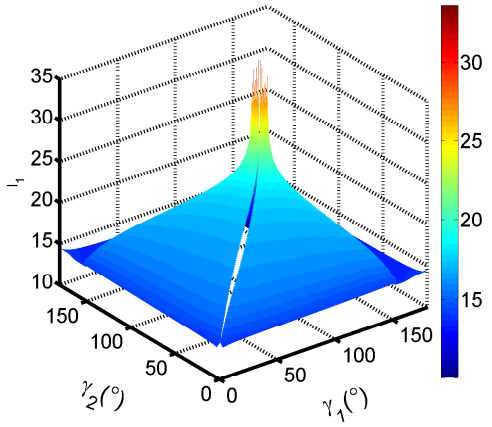

(a) performance indices I_1

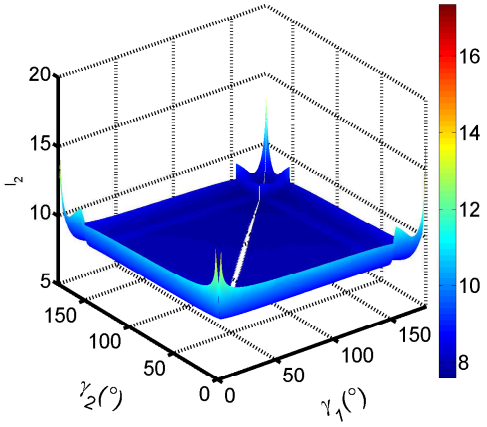

(b) performance indices I_2

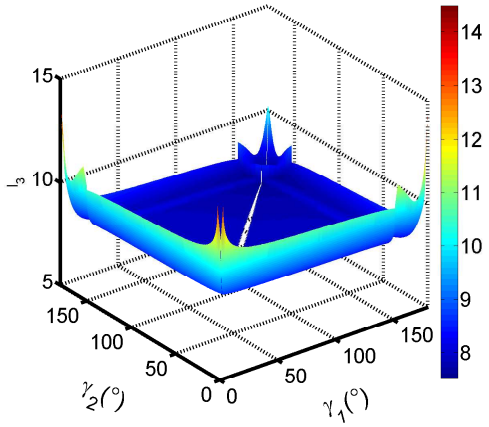

(c) performance indices I_3

Figure 3.4: The simulation results of the three observability performance indices I_1, I_2, and I_3 with respect to different polar angles, evaluated in the example uniform flow field past a Joukowski-foil-shaped robot. γ_1 is polar angle of the first sensor position and γ_2 is polar angle of the second sensor position.

Chapter 4: Simulation Example

The proposed distributed flow estimation method will be illustrated by two simulation examples, one with a uniform flow past a circular-shaped underwater robot and one with a uniform flow past a Joukowski-foil-shaped underwater robot.

4.1 Circular-shaped Underwater Robot

A circular-shaped underwater robot is used to show the effectiveness of our flow estimation method. The robot rotates about the center point of the circle in a uniform flow. The flow velocity relative to the robot is denoted as Q. We define, as shown in Fig. 4.1, an inertial reference frame I whose horizontal axis, x^I, is aligned with the direction of the flow velocity Q and its vertical axis, y^I, is perpendicular to x^I. The origin of the inertial reference frame is arbitrarily chosen to be a fixed point in the flow field. We define a body-fixed reference frame B that is attached with the underwater robot. The origin of the body-fixed frame is defined to be the center point of the circle. The horizontal axis, x^B, is along the direction that points from the head of the robot to the tail of the robot. The vertical axis, y^B, is perpendicular to x^B. The rotation angle from the x^B axis to the x^I axis is defined as the angle of attack with the counter clockwise direction as positive.

Assuming an inviscid, irrotational and incompressible fluid, we first use the potential flow theory to generate the flow field snapshots for POD model reduction [75]. The complex potential of the flow past such a circular robot is given by [85, 86]

$$F(\zeta) = Q(\zeta - \zeta_c)e^{-i\alpha} + Q\frac{R^2}{\zeta - \zeta_c}e^{i\alpha} + i\frac{\Gamma}{2\pi}\ln(\zeta - \zeta_c) \tag{4.1}$$

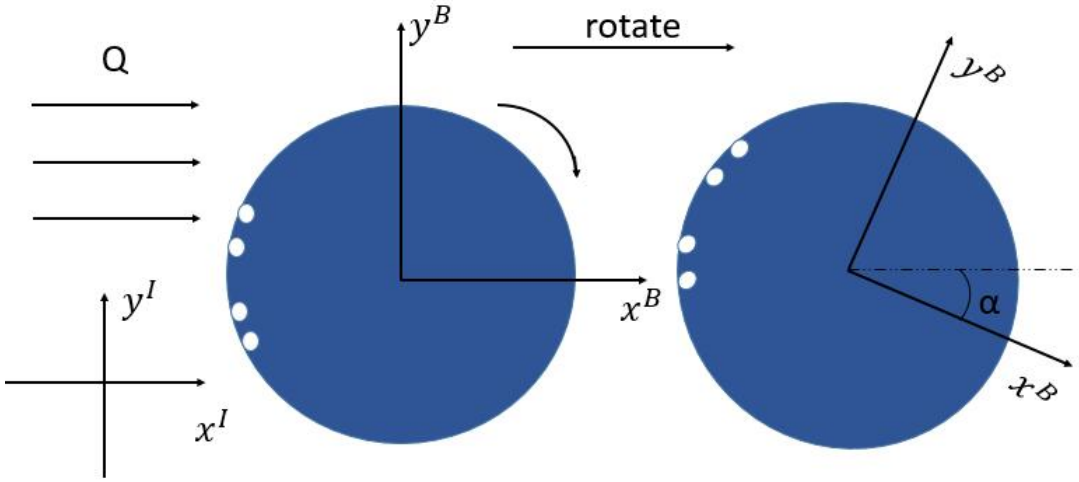

Figure 4.1: Illustration of the inertial reference frame I and the body-fixed reference frame B.

where Q is the relative flow speed, $\zeta = x + \mathrm{i}y$ is a complex number that represents the point (x, y) in the body-fixed reference frame, ζ_c is the center of the circle, R is the radius of the circle, and α is the angle of attack. The value of Γ can be found by imposing the Kutta condition that requires the trailing edge to be a stagnation point [87].

The flow velocity w is the derivative of the complex flow potential F with respect to ζ [85, 86], i.e.,

$$\begin{aligned} w(\zeta) &= \frac{dF}{d\zeta} \\ &= Qe^{-i\alpha} + Qe^{i\alpha}\frac{R^2}{(\zeta - \zeta_c)^2} + i\frac{\Gamma}{2\pi(\zeta - \zeta_c)} \end{aligned} \tag{4.2}$$

In simulation, we generate $M = 231$ velocity field snapshots using Eq. (4.2) for POD reduced-order flow modeling. The flow speed Q used in generating the snapshots ranges from 0.2 m/s to 0.4 m/s with a 0.02 m/s increment, and the angle of attack α ranges from $-20°$ to $20°$ with a $2°$ increment. Using these flow field snapshots, we calculate the optimal POD modes of the flow field. Considering jointly the computational cost and modeling

Table 4.1: The simulation results of the POD modeling percent error $\bar{E}$ for Fig. 4.2.

Time (s)	$\bar{E}$ (%)
0	3.53
1.25	0.90
2.5	1.02
3.75	1.03
5	1.02

accuracy, two POD modes are finally selected in the reduced-order flow model for the flow field around the robot.

The circular robot rotates about its center point. The angle of attack follows a sinusoidal function $\alpha = A\sin(2\pi ft)$ with the rotation amplitude A and frequency f. Designed to maximize the observability of estimated states (Section 3.3), four pressure sensors are distributed on the circular robot, shown as white dots in Fig. 4.1 with polar angles of 170° and 160° on both side. Each sensor measures the real-time local pressure. A Bayesian filter (Section 2.2) assimilates all the incoming sensor measurements and recursively estimates the two coefficients of the POD modes of the reduced-order flow model. The motion model $Pr(\wedge(t)|\wedge(t-\triangle t))$ adopts a diffusion process for the convenience of computation. Equation (2.9) then gives the flow field estimation.

Figure 4.2 shows the simulation results of the flow estimation for the circular-shaped underwater robot rotating in a uniform flow. In simulation, the rotation amplitude A is equal to 5° and the rotation frequency f is equal to 0.2 Hz. The uniform flow velocity is 0.3 m/s. The diameter of the circular robot is 5.8 cm. The sensor position vector is $\boldsymbol{z} = [-3.225 + 0.99i; -3.357 + 0.4991i; -3.357 - 0.4991i; -3.225 - 0.99i]$ and the flow measurement vector at time t is $\boldsymbol{D_c} = [\triangle\tilde{p}_{12}, \triangle\tilde{p}_{13}, \triangle\tilde{p}_{14}, \triangle\tilde{p}_{23}, \triangle\tilde{p}_{24}, \triangle\tilde{p}_{34}]^T$. The left column shows the actual velocity flow field and the right column shows the estimated velocity flow field described by the POD reduced-order flow model.

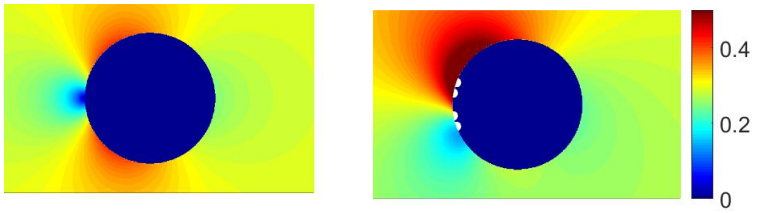

(a) $t = 0$ s, $\alpha = 0°$ (b) $t = 0$ s, $\alpha = 0°$

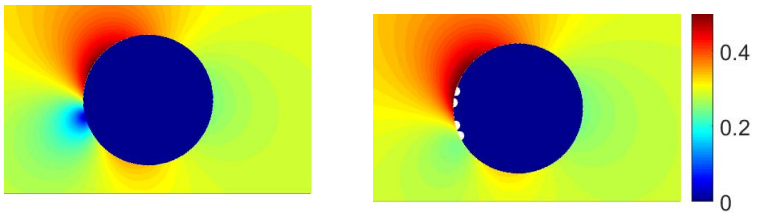

(c) $t = 1.25$ s, $\alpha = 5°$ (d) $t = 1.25$ s, $\alpha = 5°$

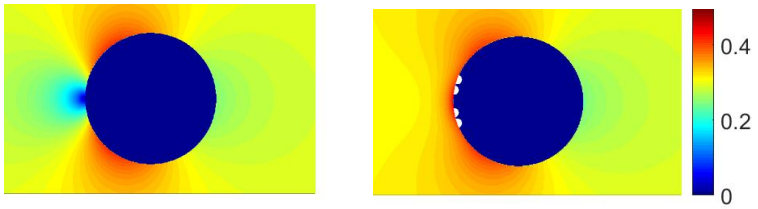

(e) $t = 2.5$ s, $\alpha = 0°$ (f) $t = 2.5$ s, $\alpha = 0°$

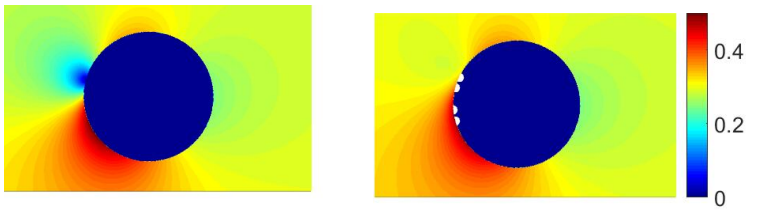

(g) $t = 3.75$ s, $\alpha = -5°$ (h) $t = 3.75$ s, $\alpha = -5°$

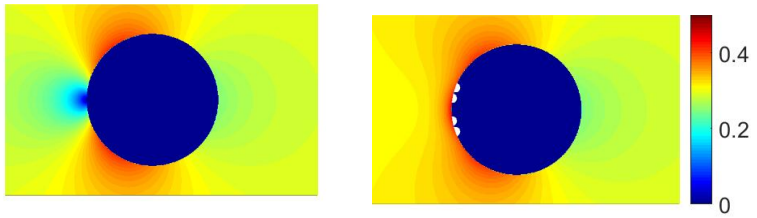

(i) $t = 5$ s, $\alpha = 0°$ (j) $t = 5$ s, $\alpha = 0°$

Figure 4.2: Simulation results of flow estimation for a circular-shaped underwater robot rotating in a uniform flow with the rotation amplitude $A = 5°$ and the rotation frequency $f = 0.2$ Hz. The left column shows the actual velocity flow field and the right column shows the estimated velocity flow field.

Table 4.1 shows the POD modeling percent error $\bar{E}$ at different time instants. The modeling percent error $\bar{E}$ is about 3.53% at first and reduces to around 1% after 1.25 s.

From Fig. 4.2 and Table. 4.1 We see that the estimated flow field approximates the actual flow field with an increasing accuracy along with time. The Bayesian filter assimilates the temporal and spatial measurements to update the probability density function of the POD coefficients. More measurement data of the flow leads to better estimation accuracy and the estimation error converges to 1% eventually. With the existence of flow model reduction errors and sensor measurement noises, we consider the flow estimation results satisfactory.

4.2 Joukowski-foil-shaped Underwater Robot

In this section, we apply the proposed distributed flow estimation approach on a Joukowski-foil-shaped underwater robot. The shape is defined as the output image of the Joukowski transformation, which is a conformal mapping commonly used in airfoil design [88]. Through the potential flow theory, we calculate the complex potential of the flow field as a function of the flow speed and the angle of attack [2,40,71,73,75,85,89]. The gradient of the complex potential gives the flow velocity.

In simulation, we use a robot with a length of 19.2 cm and a width of 3.8 cm. The underwater robot is equipped with four pressure sensors with two on each side, shown as white dots in Fig. 4.3. The sensor placement follows the strategy as discussed in Section 3.3. The sensor position vector is $\boldsymbol{z} = [-4.8572 + 0.4889i; -5.0357 + 0.2495i; -5.0357 - 0.2495i; -4.8572 - 0.4889i]^{\mathrm{T}}$. The robot rotates in a uniform flow with its angle of attack following a sinusoidal function $\alpha = A\sin(2\pi ft)$. We generate $M = 231$ velocity field snapshots using potential flow theory and calculate the optimal POD modes for the flow field. The flow speed used to generate the flow field snapshot ranges from 0.2 m/s to 0.4 m/s with a 0.02 m/s discretization step. The angle of attack ranges from $-20°$ to $-20°$ with a $2°$ discretization step. Two POD modes are selected for the reduced-order flow model. The motion model $Pr(\wedge(t)|\wedge(t-\triangle t))$ adopts a diffusion process.

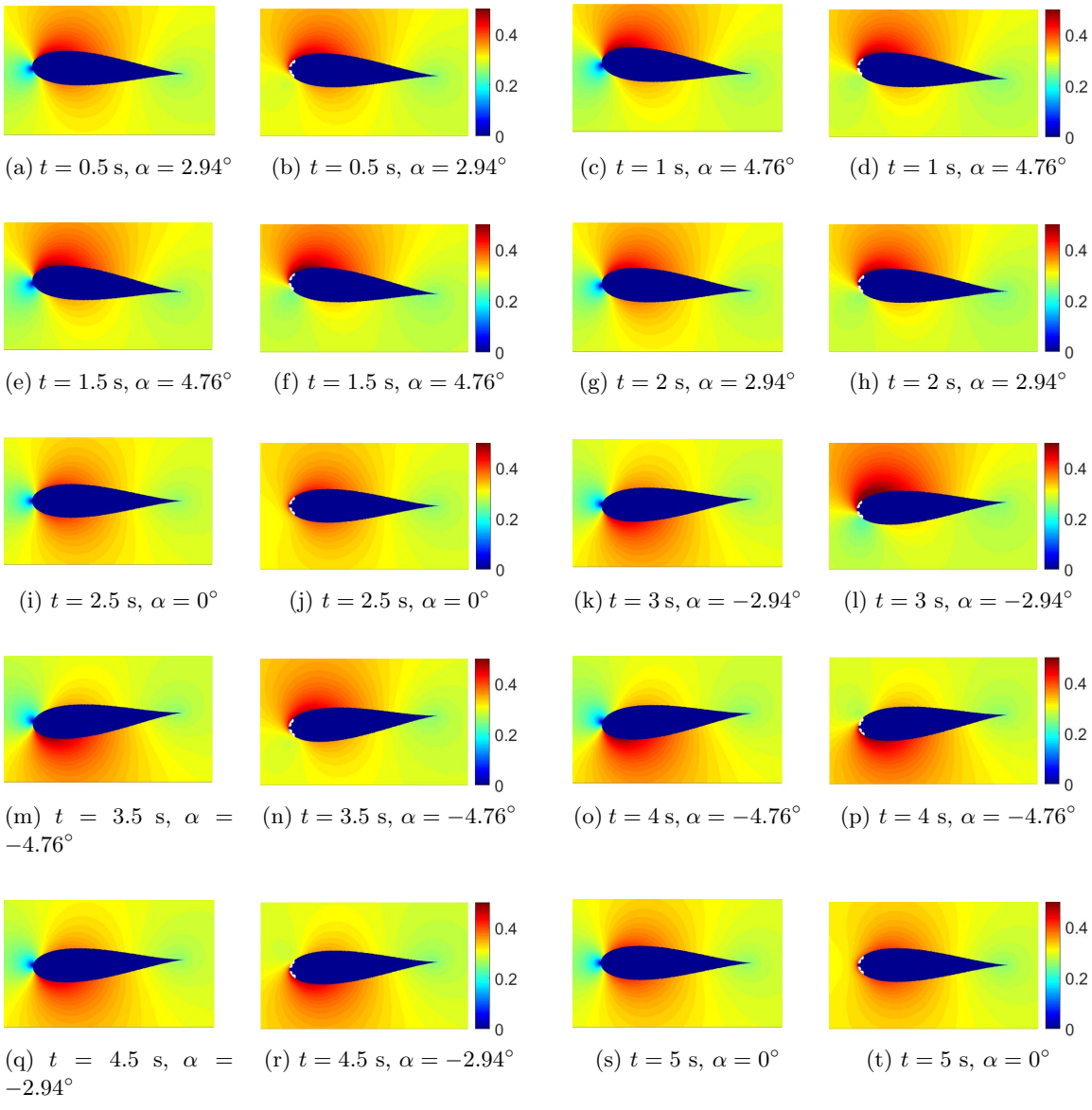

(a) $t = 0.5$ s, $\alpha = 2.94°$ (b) $t = 0.5$ s, $\alpha = 2.94°$ (c) $t = 1$ s, $\alpha = 4.76°$ (d) $t = 1$ s, $\alpha = 4.76°$

(e) $t = 1.5$ s, $\alpha = 4.76°$ (f) $t = 1.5$ s, $\alpha = 4.76°$ (g) $t = 2$ s, $\alpha = 2.94°$ (h) $t = 2$ s, $\alpha = 2.94°$

(i) $t = 2.5$ s, $\alpha = 0°$ (j) $t = 2.5$ s, $\alpha = 0°$ (k) $t = 3$ s, $\alpha = -2.94°$ (l) $t = 3$ s, $\alpha = -2.94°$

(m) $t = 3.5$ s, $\alpha = -4.76°$ (n) $t = 3.5$ s, $\alpha = -4.76°$ (o) $t = 4$ s, $\alpha = -4.76°$ (p) $t = 4$ s, $\alpha = -4.76°$

(q) $t = 4.5$ s, $\alpha = -2.94°$ (r) $t = 4.5$ s, $\alpha = -2.94°$ (s) $t = 5$ s, $\alpha = 0°$ (t) $t = 5$ s, $\alpha = 0°$

Figure 4.3: Simulation results of flow estimation for a Joukowski-foil-shaped underwater robot rotating in a uniform flow with the rotation amplitude $A = 5°$ and the rotation frequency $f = 0.2$ Hz. The first and third column shows the actual velocity flow field. The second and fourth column shows the estimated velocity flow field.

Table 4.2: The simulation results of the POD modeling percent error $\bar{E}$ for the Fig. 4.3.

Time (s)	$\bar{E}$ (%)
0	26.9
0.5	1
1	0.94
1.5	0.94
2	1.15
2.5	1.15
3	3.44
3.5	2.86
4	0.87
4.5	0.98
5	1.02

Figure 4.3 shows the simulation results of distributed flow estimation of the Joukowski-foil-shaped underwater robot rotating in a uniform flow with a constant flow velocity of 0.3 m/s. Table 4.2 shows the POD modeling percent error $\bar{E}$ at different time instants. From 0.5 s to 2.5 s, $\bar{E}$ is nearly 1% and grows larger at 3 s to about 3.44%. That's when the fish rotates through zero angle of attack. After 4 s, $\bar{E}$ returns to about 1% and maintains at that level. We conjecture the growing in the error comes from a rapid rotating movement of the robot around zero angle of attack, which challenges the assumption of the quasi-steady flow conditions. With the existence of flow model reduction errors and sensor measurement noises, we consider the estimation error satisfactory.

Chapter 5: Application in Angle-of-Attack Control of Robotic Fish

This section presents the application of the proposed flow estimation method in the closed-loop control of underwater robots. The design idea is illustrated by the simulation results of the angle-of-attack regulation of a Joukowski-foil-shaped robot.

5.1 Flow Estimation Based Angle-of-Attack Regulation

Using their lateral line systems, fish tend to turn against flow currents for station holding to save energy [72, 90]. In this thesis, we will use the angle-of-attack regulation as an example to demonstrate the application of the proposed flow estimation approach in closed-loop control of underwater robots. The control objective is to regulate a Joukowski-foil-shaped underwater robot to stay at zero degree of angle of attack in a uniform flow using distributed flow estimation feedback [46, 47].

We adopt a commonly-used simplified rotational dynamics model for a Joukowski-shaped underwater robot [46], i.e.,

$$J\dot{\Omega} = T_p - T_c \tag{5.1}$$

where J is the inertia of the robot including the added inertia in the rotational direction, Ω is the angular velocity of underwater robot, T_c is the control torque and T_p is the hydrodynamic moment given by [91]

$$T_p = C_p \alpha Q^2 - K_p \Omega \tag{5.2}$$

where Q is the flow-relative speed of the robot, C_p is the hydrodynamic moment coefficient and K_p is the damping coefficient. The positive direction of the angular velocity Ω is defined as counter-clockwise, opposite to the direction of the changing rate of the angle of attack α, i.e.,

$$\dot{\alpha} = -\Omega \tag{5.3}$$

We adopt a PID controller for the angle of attack regulation. The block diagram of the closed-loop system is shown in Fig. 5.1.

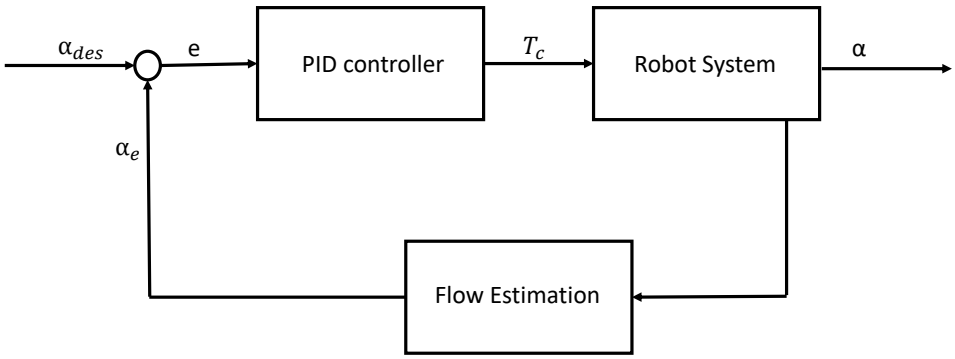

Figure 5.1: The block diagram of the closed-loop control of the angle of attack using flow estimation feedback for an underwater robot.

The PID controller is given by

$$T_c = K_1 e + K_2 \int e \mathrm{d}t + K_3 \frac{\mathrm{d}e}{\mathrm{d}t} \tag{5.4}$$

where T_c is the control torque used to control the rotation motion of underwater robot, $e = \alpha_{des} - \alpha_e$ is the difference between the desired and estimated angle of attack. K_1, K_2, and K_3 are the PID controller coefficients. The feedback angle of attack is obtained from estimated flow using the neural network model discussed in Section 3.2.

5.2 Simulation Results

In simulation, we used four POD modes to model the flow field following the POD mode selection analysis in Section 3.1 for a balance between modeling error and computation effort in angle-of-attack regulation. Figure 5.2 shows the simulated four optimal POD modes of the reduced-order flow model. The first mode represents the major component of the flow field around underwater robot. The remaining ones add more detailed features to the flow field.

These four optimal POD modes are used to construct the POD reduced order flow model, based on which we calculate the likelihood function of the Bayesian filter and estimate the flow parameters. The angle of attack estimation is then calculated using the neural network introduced in Section 3.2. We adopt a three-layer neural network with 10 nodes in the hidden layer to establish the relationship between POD mode coefficients and the angle of attack. The original 231 flow field snapshots and their POD mode coefficients are used to train the neural network. The details of the parameters are as shown below.

The parameters of this neural network is shown below:

1. The input are the POD coefficients.
2. The output is the angle of attack.
3. The transfer function of the hidden layer is hyperbolic tangent sigmoid transfer function ("tansig()")
4. The transfer function of the output layer is linear transfer function ("purelin()")
5. The train function is a network training function that updates weight and bias values according to Levenberg-Marquardt optimization. It is often the fastest backpropagation algorithm in the toolbox, and is highly recommended as a first-choice supervised algorithm, although it does require more memory than other algorithms. ("trainlm()")

The structure of the neural network used in mapping the POD coefficients are shown in Fig. 5.3.

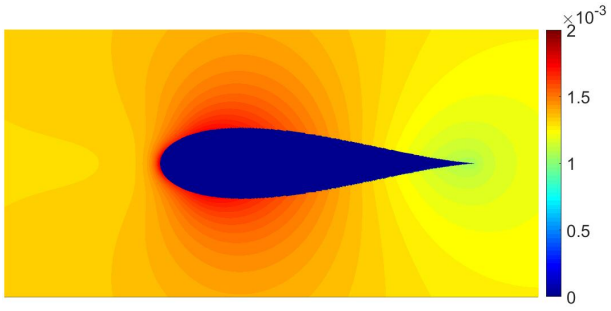

(a) first POD mode

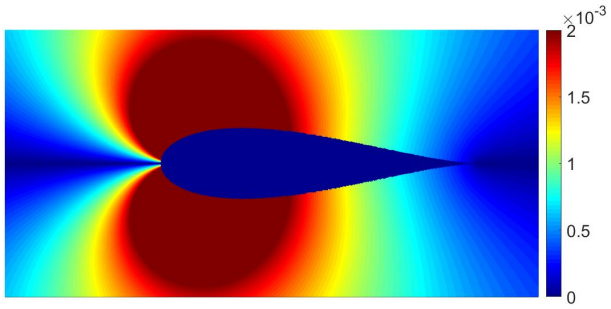

(b) second POD mode

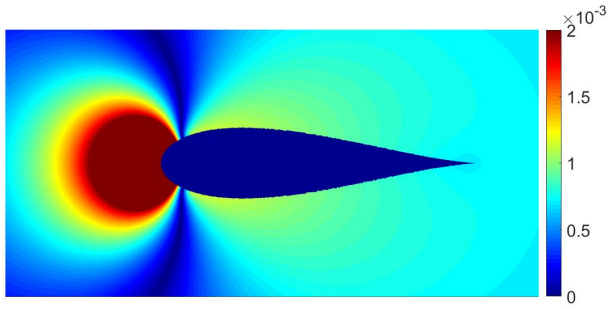

(c) third POD mode

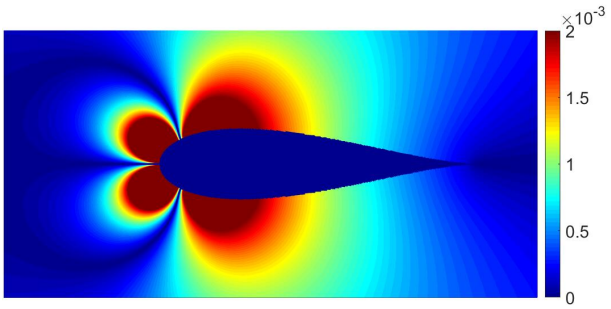

(d) fourth POD mode

Figure 5.2: The simulation results of the four optimal POD modes in the reduced-order flow model on the velocity flow fields. The color map shows the distribution of the flow velocity in the unit of m/s.

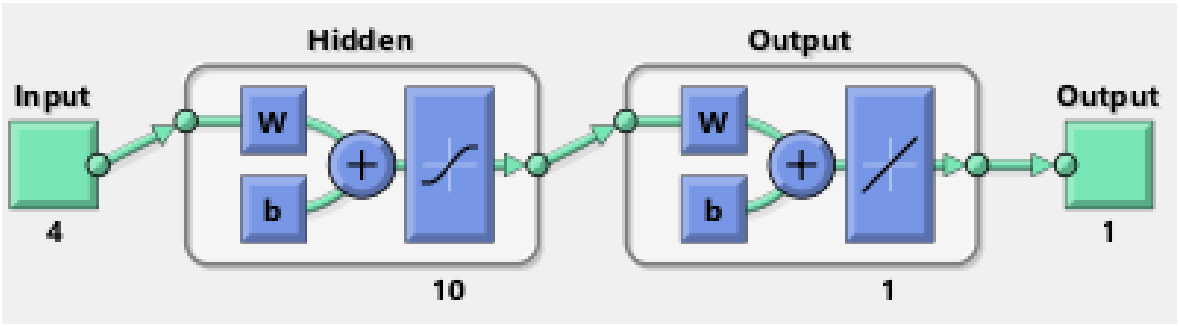

Figure 5.3: The neural network structure used in angle of attack control of the Joukowski-foil-shaped underwater robot.

Figure 5.4 shows that the estimated angle of attack follows the trajectory of the actual angle of attack reasonably well in a testing case study where the actual angle of attack follows a sinusoidal function.

Using a PID controller (5.4), we simulated the closed-loop angle-of-attack regulation with the initial condition of the angle of attack at 5°. The parameters of the dynamic system used in simulation are $C_p = 1$ kg, $K_p = 1$ kg.

In simulation, we assume the sensor noise level is 10% of pressure measurements. Figure 5.5 shows the simulation results on the trajectory of the angle of attack. The color map shows the marginal probability density of the estimated angle of attack. The estimated value is selected to be the point in the estimation space with the highest probability density. First the results show that the estimated angle of attack match with the actual value sufficiently well. Second, we see that the angle of attack converges to near 0° within 7 seconds with the closed-loop control. We consider the angle-of-attack regulation satisfactory, especially considering the sensor measurement noise and the modeling error in the POD flow model reduction.

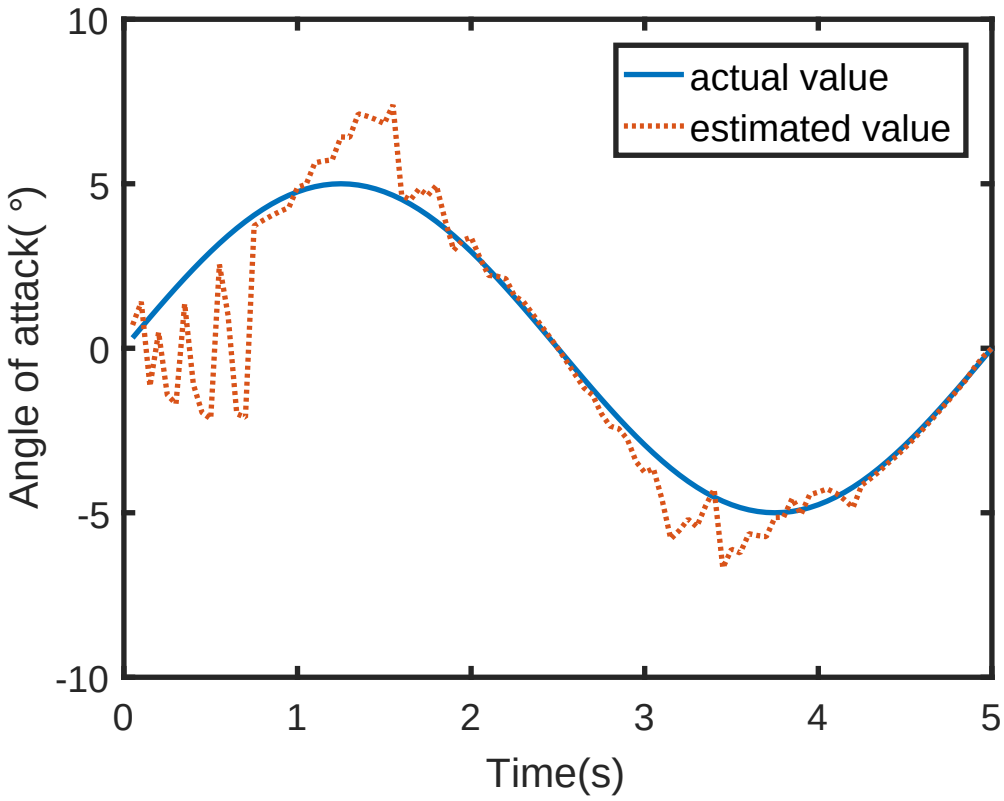

Figure 5.4: The trajectories of the actual (blue line) and estimated (red line) angle of attack of the Joukowski-foil-shaped underwater robot.

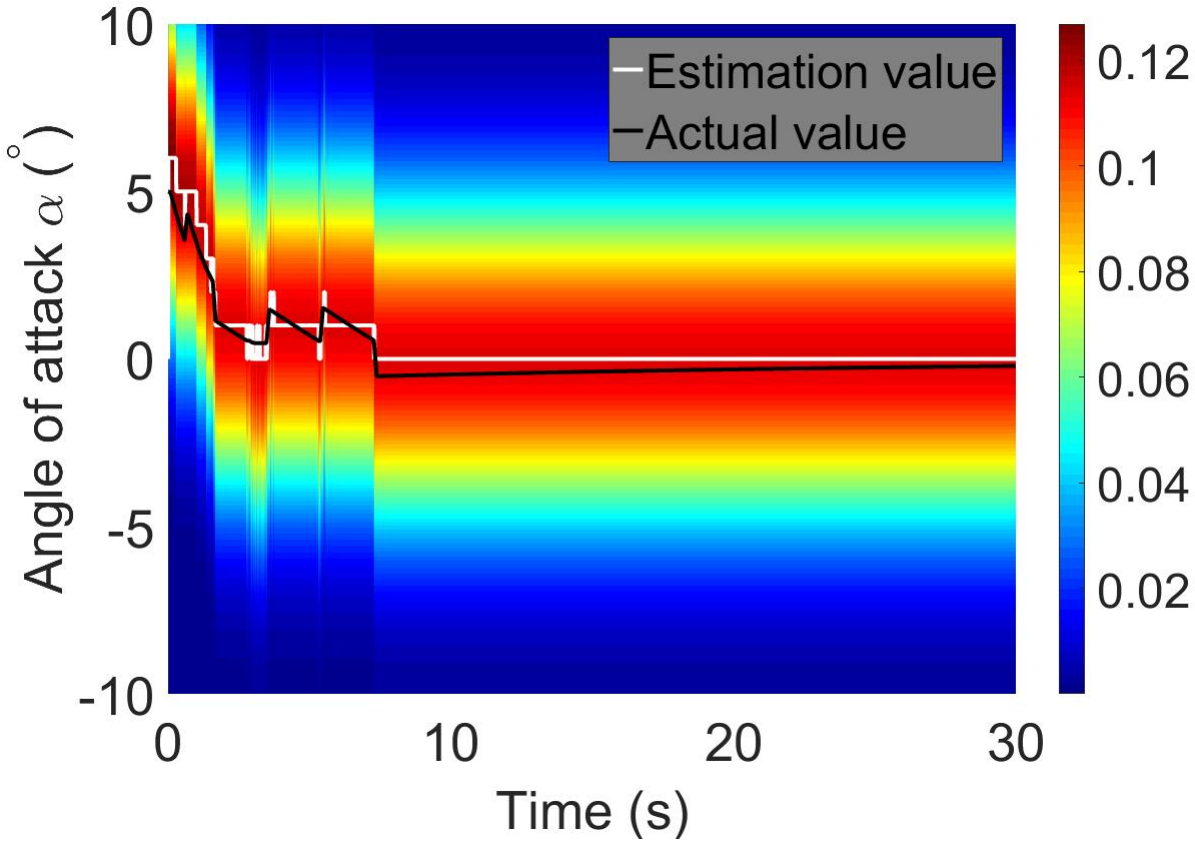

Figure 5.5: The simulated trajectory of the angle of attack of the underwater robot in the closed-loop system.

Chapter 6: Conclusion

This thesis proposed a new method of distributed flow estimation for autonomous underwater robots, which integrates a Bayesian filter and a POD-based reduced-order flow model. There are three important problems which affect the algorithm's performance, POD flow model reduction accuracy, relationship between the POD coefficients and conventional flow parameters, and the distributed sensor placement strategy. So we quantitatively analyzed and discussed the POD flow model reduction accuracy, relationship between the POD coefficients and conventional flow parameters, and the distributed sensor placement strategy. We found the more POD modes will increase POD flow model reduction accuracy. However the computation need to be considered at the same time. A three layer neural network is used to approximate angle of attack using POD modes coefficients. A Gramian matrix is used to help decide the sensor position and get a good coefficients observability.

For the validation of the proposed flow estimation approach, a cylinder-shaped underwater robot and a Joukowski-foil-shaped underwater robot were used as examples in simulation. Based on this, a closed-loop angle-of-attack regulation system was also studied using the estimated flow as feedback. PID controller is used in this process to regulate the angle of attack and make it converge to near 0$\circ$ within 7 seconds with the closed-loop control. The simulation results showed that the angle-of-attack regulation was satisfactory which further validated the effectiveness of the proposed flow estimation in real-time control of autonomous underwater robots.

In future work, we will experimentally evaluate the proposed model-reduction-based flow estimation method with an custom-designed flow sensing underwater robot.

Bibliography

[1] P. R. Bandyopadhyay, "Trends in biorobotic autonomous undersea vehicles," *IEEE Journal of Oceanic Engineering*, vol. 30, no. 1, pp. 109–139, 2005.

[2] F. Zhang, O. Ennasr, E. Litchman, and X. Tan, "Autonomous sampling of water columns using gliding robotic fish: Algorithms and harmful-algae-sampling experiments," *IEEE Systems Journal*, vol. 10, no. 3, pp. 1271–1281, 2016.

[3] A. Wolek, T. Gode, C. A. Woolsey, J. Quenzer, and K. A. Morgansen, "Testing a pneumatic underwater glider in shallow water," in *OCEANS'15 MTS/IEEE Washington*. IEEE, 2015, pp. 1–8.

[4] P. Phamduy, J. Cheong, and M. Porfiri, "An autonomous charging system for a robotic fish," *IEEE/ASME Transactions on Mechatronics*, vol. 21, no. 6, pp. 2953–2963, 2016.

[5] B. R. Page, S. Ziaeefard, A. J. Pinar, and N. Mahmoudian, "Highly maneuverable low-cost underwater glider: Design and development," *IEEE Robotics and Automation Letters*, vol. 2, no. 1, pp. 344–349, 2017.

[6] D. Rus and M. T. Tolley, "Design, fabrication and control of soft robots," *Nature*, pp. 467–475, 2015.

[7] D. S. Barrett, "Propulsive efficiency of a flexible hull underwater vehicle," Ph.D. dissertation, Massachusetts Institute of Technology, 1996.

[8] R. Ding, J. Yu, Q. Yang, M. Tan, and J. Zhang, "Cpg-based dynamics modeling and simulation for a biomimetic amphibious robot," in *Robotics and Biomimetics (ROBIO), 2009 IEEE International Conference on*. IEEE, 2009, pp. 1657–1662.

[9] B. P. Epps, P. V. y Alvarado, K. Youcef-Toumi, and A. H. Techet, "Swimming performance of a biomimetic compliant fish-like robot," *Experiments in fluids*, vol. 47, no. 6, p. 927, 2009.

[10] R. Fan, J. Yu, L. Wang, G. Xie, Y. Fang, and Y. Hu, "Optimized design and implementation of biomimetic robotic dolphin," in *Robotics and Biomimetics (ROBIO). 2005 IEEE International Conference on*. IEEE, 2005, pp. 484–489.

[11] K. Hirata *et al.*, "Development of experimental fish robot," in *Sixth International Symposium on Marine Engineering (ISME 2000), Tokyo, Japan, Oct*, 2000, pp. 23–27.

[12] K. Hirata, T. Takimoto, and K. Tamura, "Study on turning performance of a fish robot," in *First International Symposium on Aqua Bio-Mechanisms*, 2000, pp. 287–292.

[13] H. Hu, "Biologically inspired design of autonomous robotic fish at essex," in *IEEE SMC UK-RI Chapter Conference, on Advances in Cybernetic Systems*. Citeseer, 2006, pp. 3–8.

[14] J.-D. Liu and H. Hu, "Biologically inspired behaviour design for autonomous robotic fish," *International Journal of Automation and Computing*, vol. 3, no. 4, pp. 336–347, 2006.

[15] Y. Hu, L. Wang, J. Yu, J. Huo, and Y. Jia, "Development and control of dolphin-like underwater vehicle," in *American Control Conference, 2008*. IEEE, 2008, pp. 2858–2863.

[16] A. Konno, T. Furuya, A. Mizuno, K. Hishinuma, K. Hirata, and M. Kawada, "Development of turtle-like submersible vehicle," *Marine Engineering*, vol. 41, no. SI, pp. 158–163, 2006.

[17] D. Lachat, A. Crespi, and A. J. Ijspeert, "Boxybot: a swimming and crawling fish robot controlled by a central pattern generator," in *Proceedings of the first IEEE/RAS-EMBS international conference on biomedical robotics and biomechatronics (BioRob 2006)*, no. BIOROB-CONF-2006-010, 2006.

[18] K. Low and C. Chong, "Parametric study of the swimming performance of a fish robot propelled by a flexible caudal fin," *Bioinspiration & Biomimetics*, vol. 5, no. 4, p. 046002, 2010.

[19] E. Papadopoulos, E. Apostolopoulos, and P. Tsigkourakos, "Design, control, and experimental performance of a teleoperated robotic fish," in *Control and Automation, 2009. MED'09. 17th Mediterranean Conference on*. IEEE, 2009, pp. 766–771.

[20] W. Wang, J. Yu, R. Ding, and M. Tan, "Bio-inspired design and realization of a novel multimode amphibious robot," in *Automation and Logistics, 2009. ICAL'09. IEEE International Conference on*. IEEE, 2009, pp. 140–145.

[21] C. Zhou and K. Low, "Design and locomotion control of a biomimetic underwater vehicle with fin propulsion," *IEEE/ASME Transactions on Mechatronics*, vol. 17, no. 1, pp. 25–35, 2012.

[22] T. I. Fossen, *Guidance and control of ocean vehicles*. John Wiley & Sons Inc, 1994.

[23] J. Yuh, "Modeling and control of underwater robotic vehicles," *IEEE Transactions on Systems, man, and Cybernetics*, vol. 20, no. 6, pp. 1475–1483, 1990.

[24] K. Goheen, "Modeling methods for underwater robotic vehicle dynamics," *Journal of Robotic Systems*, vol. 8, no. 3, pp. 295–317, 1991.

[25] F. Fnaiech and L. Ljung, "Recursive identification of bilinear systems," *International journal of control*, vol. 45, no. 2, pp. 453–470, 1987.

[26] A. Alessandri, M. Caccia, G. Indiveri, and G. Veruggio, "Application of ls and ekf techniques to the identification of underwater vehicles," in *Control Applications, 1998. Proceedings of the 1998 IEEE International Conference on*, vol. 2. IEEE, 1998, pp. 1084–1088.

[27] J. G. Balchen, N. A. Jenssen, E. Mathisen, and S. Sælid, "Dynamic positioning of floating vessles based on kalman filtering and optimal control," in *Decision and Control including the Symposium on Adaptive Processes, 1980 19th IEEE Conference on.* IEEE, 1980, pp. 852–864.

[28] T. I. Fossen, S. I. Sagatun, and A. J. Sørensen, "Identification of dynamically positioned ships," *Control Engineering Practice*, vol. 4, no. 3, pp. 369–376, 1996.

[29] P. Ridao, A. Tiano, A. El-Fakdi, M. Carreras, and A. Zirilli, "On the identification of non-linear models of unmanned underwater vehicles," *Control engineering practice*, vol. 12, no. 12, pp. 1483–1499, 2004.

[30] P. W. Van De Ven, T. A. Johansen, A. J. Sørensen, C. Flanagan, and D. Toal, "Neural network augmented identification of underwater vehicle models," *Control Engineering Practice*, vol. 15, no. 6, pp. 715–725, 2007.

[31] A. Tiano, R. Sutton, A. Lozowicki, and W. Naeem, "Observer kalman filter identification of an autonomous underwater vehicle," *Control engineering practice*, vol. 15, no. 6, pp. 727–739, 2007.

[32] M. A. Abkowitz, "Measurement of hydrodynamic characteristics from ship maneuvering trials by system identification," Tech. Rep., 1980.

[33] H. L. Brinati, "System identification applied to maneuvering trials," Tech. Rep., 1973.

[34] R. G. Brown and P. Y. Hwang, "Introduction to random signals and applied kalman filtering: with matlab exercises and solutions," *Introduction to random signals and applied Kalman filtering: with MATLAB exercises and solutions, by Brown, Robert Grover.; Hwang, Patrick YC New York: Wiley, c1997.*, 1997.

[35] W.-Y. Hwang, "Application of system identification to ship maneuvering," Ph.D. dissertation, Massachusetts Institute of Technology, 1980.

[36] J. G. Lundblad, "Application of the extended kalman filtering technique to ship maneuvering analysis," Tech. Rep., 1975.

[37] T. Moran, A. Wemple, and W. Smith, "Mariner surface ship system identification," 1984.

[38] H. K. Yoon and K. P. Rhee, "Identification of hydrodynamic coefficients in ship maneuvering equations of motion by estimation-before-modeling technique," *Ocean Engineering*, vol. 30, no. 18, pp. 2379–2404, 2003.

[39] L. DeVries, F. D. Lagor, H. Lei, X. Tan, and D. A. Paley, "Distributed flow estimation and closed-loop control of an underwater vehicle with a multi-modal artificial lateral line," *Bioinspiration & biomimetics*, vol. 10, no. 2, p. 025002, 2015.

[40] F. Dang and F. Zhang, "Identification of hydrodynamic coefficients of a robotic fish using improved extended kalman filter," in *ASME 2017 Dynamic Systems and Control Conference.* American Society of Mechanical Engineers, 2017, pp. V001T30A012–V001T30A012.

[41] F. Zhang, F. D. Lagor, D. Yeo, P. Washington, and D. A. Paley, "Distributed flow sensing using bayesian estimation for a flexible fish robot," in *ASME 2015 Dynamic Systems and Control Conference*. American Society of Mechanical Engineers, 2015, pp. V002T23A004–V002T23A004.

[42] A. Gao and M. Triantafyllou, *Bio-inspired pressure sensing for active yaw control of underwater vehicles*. IEEE, 2012.

[43] V. I. Fernandez, A. Maertens, F. M. Yaul, J. Dahl, J. H. Lang, and M. S. Triantafyllou, "Lateral-line-inspired sensor arrays for navigation and object identification," *Marine Technology Society Journal*, vol. 45, no. 4, pp. 130–146, 2011.

[44] A. Kohl, K. Y. Pettersen, E. Kelasidi, and J. T. Gravdahl, "Planar path following of underwater snake robots in the presence of ocean currents," *IEEE Robotics and Automation Letters*, vol. 1, no. 1, pp. 383–390, 2016.

[45] Y. Xu and K. Mohseni, "A pressure sensory system inspired by the fish lateral line: Hydrodynamic force estimation and wall detection," *IEEE Journal of Oceanic Engineering*, vol. 42, no. 3, pp. 532–543, 2017.

[46] F. Zhang, P. Washington, and D. A. Paley, "A flexible, reaction-wheel-driven fish robot: Flow sensing and flow-relative control," in *American Control Conference (ACC), 2016*. IEEE, 2016, pp. 1221–1226.

[47] F. D. Lagor, L. D. DeVries, K. Waychoff, and D. A. Paley, "Bio-inspired flow sensing and control: Autonomous rheotaxis using distributed pressure measurements," *Journal of Unmanned System Technology*, vol. 1, no. 3, pp. 78–88, 2013.

[48] J. B. Sousa, F. L. Pereira, P. Souto, L. Madureira, and E. P. Da Silva, "Distributed sensor and vehicle networked systems for environmental applications," in *Proceedings of the Environment 2010: Situation and Perspectives for the European Union Conference*, 2003.

[49] Z. Wang, G. Hang, Y. Wang, J. Li, and W. Du, "Embedded sma wire actuated biomimetic fin: a module for biomimetic underwater propulsion," *Smart Materials and Structures*, vol. 17, no. 2, p. 025039, 2008.

[50] Z. Wang, Y. Wang, J. Li, and G. Hang, "A micro biomimetic manta ray robot fish actuated by sma," in *Robotics and Biomimetics (ROBIO), 2009 IEEE International Conference on*. IEEE, 2009, pp. 1809–1813.

[51] H. Kim, "Smart soft-morphing structure: design, manufacturing, and application," Ph.D. dissertation, Ph. D. Thesis, School of Mechanical and Aerospace Engineering, Seoul National University, 2011.

[52] S.-H. Ahn, K.-T. Lee, H.-J. Kim, R. Wu, J.-S. Kim, and S.-H. Song, "Smart soft composite: An integrated 3d soft morphing structure using bend-twist coupling of anisotropic materials," *International Journal of Precision Engineering and Manufacturing*, vol. 13, no. 4, pp. 631–634, 2012.

[53] L. Shi, S. Guo, and K. Asaka, "A novel jellyfish-like biomimetic microrobot," in *Complex Medical Engineering (CME), 2010 IEEE/ICME International Conference on*. IEEE, 2010, pp. 277–281.

[54] S.-W. Yeom and I.-K. Oh, "A biomimetic jellyfish robot based on ionic polymer metal composite actuators," *Smart materials and structures*, vol. 18, no. 8, p. 085002, 2009.

[55] M. Aureli, V. Kopman, and M. Porfiri, "Free-locomotion of underwater vehicles actuated by ionic polymer metal composites," *IEEE/ASME transactions on mechatronics*, vol. 15, no. 4, pp. 603–614, 2010.

[56] Z. Chen, S. Shatara, and X. Tan, "Modeling of biomimetic robotic fish propelled by an ionic polymer–metal composite caudal fin," *IEEE/ASME transactions on mechatronics*, vol. 15, no. 3, pp. 448–459, 2010.

[57] W. Yim, J. Lee, and K. J. Kim, "An artificial muscle actuator for biomimetic underwater propulsors," *Bioinspiration & biomimetics*, vol. 2, no. 2, p. S31, 2007.

[58] S. Heo, T. Wiguna, H. C. Park, and N. S. Goo, "Effect of an artificial caudal fin on the performance of a biomimetic fish robot propelled by piezoelectric actuators," *Journal of Bionic Engineering*, vol. 4, no. 3, pp. 151–158, 2007.

[59] Y. Yang, X. Ye, and S. Guo, "A new type of jellyfish-like microrobot," in *Integration Technology, 2007. ICIT'07. IEEE International Conference on*. IEEE, 2007, pp. 673–678.

[60] S. Guo, L. Shi, X. Ye, and L. Li, "A new jellyfish type of underwater microrobot," in *Mechatronics and Automation, 2007. ICMA 2007. International Conference on*. IEEE, 2007, pp. 509–514.

[61] M. Norgia, A. Pesatori, and L. Rovati, "Self-mixing laser doppler spectra of extracorporeal blood flow: a theoretical and experimental study," *IEEE Sensors Journal*, vol. 12, no. 3, pp. 552–557, 2012.

[62] A. Forrest, R. Cossu, Z. Leong, D. Ranmuthugala *et al.*, "Estimating flow velocities of the water column using the motion response of an autonomous underwater vehicle (auv)," in *OCEANS'15 MTS/IEEE Washington*. IEEE, 2015, pp. 1–6.

[63] Z. Fan, J. Chen, J. Zou, D. Bullen, C. Liu, and F. Delcomyn, "Design and fabrication of artificial lateral line flow sensors," *Journal of micromechanics and microengineering*, vol. 12, no. 5, p. 655, 2002.

[64] Y. Yang, J. Chen, J. Engel, S. Pandya, N. Chen, C. Tucker, S. Coombs, D. L. Jones, and C. Liu, "Distant touch hydrodynamic imaging with an artificial lateral line," *Proceedings of the National Academy of Sciences*, vol. 103, no. 50, pp. 18 891–18 895, 2006.

[65] N. Svedin, E. Stemme, and G. Stemme, "A static turbine flow meter with a micromachined silicon torque sensor," *Journal of microelectromechanical systems*, vol. 12, no. 6, pp. 937–946, 2003.

[66] A. Klein and H. Bleckmann, "Determination of object position, vortex shedding frequency and flow velocity using artificial lateral line canals," *Beilstein journal of nanotechnology*, vol. 2, p. 276, 2011.

[67] L. Campagnolo, M. Nikolić, J. Perchoux, Y. L. Lim, K. Bertling, K. Loubiere, L. Prat, A. D. Rakić, and T. Bosch, "Flow profile measurement in microchannel using the optical feedback interferometry sensing technique," *Microfluidics and Nanofluidics*, vol. 14, no. 1-2, pp. 113–119, 2013.

[68] A. G. Kottapalli, M. Asadnia, J. Miao, G. Barbastathis, and M. S. Triantafyllou, "A flexible liquid crystal polymer mems pressure sensor array for fish-like underwater sensing," *Smart Materials and Structures*, vol. 21, no. 11, p. 115030, 2012.

[69] A. Kottapalli, C. Tan, M. Olfatnia, J. Miao, G. Barbastathis, and M. Triantafyllou, "A liquid crystal polymer membrane mems sensor for flow rate and flow direction sensing applications," *Journal of Micromechanics and Microengineering*, vol. 21, no. 8, p. 085006, 2011.

[70] L. DeVries and D. A. Paley, "Observability-based optimization for flow sensing and control of an underwater vehicle in a uniform flowfield," in *American Control Conference (ACC), 2013*. IEEE, 2013, pp. 1386–1391.

[71] F. Zhang, F. D. Lagor, D. Yeo, P. Washington, and D. A. Paley, "Distributed flow sensing for closed-loop speed control of a flexible fish robot," *Bioinspiration & biomimetics*, vol. 10, no. 6, p. 065001, 2015.

[72] S. Coombs, "Smart skins: information processing by lateral line flow sensors," *Autonomous Robots*, vol. 11, no. 3, pp. 255–261, 2001.

[73] F. Zhang, F. D. Lagor, D. Yeo, P. Washington, and D. A. Paley, "Distributed flow sensing using bayesian estimation for a flexible fish robot," in *ASME 2015 Dynamic Systems and Control Conference*. American Society of Mechanical Engineers, 2015, pp. V002T23A004–V002T23A004.

[74] T. Kurahashi, K. Saito, and M. Nogami, "Application of the ensemble kalman filter fem for estimation of flow field in shallow water regions," *JSIAM Letters*, vol. 10, pp. 5–8, 2015.

[75] J. L. Lumley, "Computational modeling of turbulent flows," in *Advances in applied mechanics*. Elsevier, 1979, vol. 18, pp. 123–176.

[76] G. K. Batchelor, *An introduction to fluid dynamics*. Cambridge university press, 2000.

[77] M. R. Jovanović, P. J. Schmid, and J. W. Nichols, "Sparsity-promoting dynamic mode decomposition," *Physics of Fluids*, vol. 26, no. 2, p. 024103, 2014.

[78] M. Gad-el Hak, "The fluid mechanics of microdevices—the freeman scholar lecture," *Journal of Fluids Engineering*, vol. 121, no. 1, pp. 5–33, 1999.

[79] S. M. Ross, *Introduction to probability models*. Academic press, 2014.

[80] M. Eslami, *Theory of sensitivity in dynamic systems: an introduction.* Springer Science & Business Media, 2013.

[81] S. Haykin and N. Network, "A comprehensive foundation," *Neural networks*, vol. 2, no. 2004, p. 41, 2004.

[82] J. Ni, L. Wu, P. Shi, and S. X. Yang, "A dynamic bioinspired neural network based real-time path planning method for autonomous underwater vehicles," *Computational intelligence and neuroscience*, vol. 2017, 2017.

[83] J. Gao, A. A. Proctor, Y. Shi, and C. Bradley, "Hierarchical model predictive image-based visual servoing of underwater vehicles with adaptive neural network dynamic control," *IEEE transactions on cybernetics*, vol. 46, no. 10, pp. 2323–2334, 2016.

[84] A. J. Krener and K. Ide, "Measures of unobservability," in *Decision and Control, 2009 held jointly with the 2009 28th Chinese Control Conference. CDC/CCC 2009. Proceedings of the 48th IEEE Conference on.* IEEE, 2009, pp. 6401–6406.

[85] F. H. Harlow and J. E. Welch, "Numerical calculation of time-dependent viscous incompressible flow of fluid with free surface," *The physics of fluids*, vol. 8, no. 12, pp. 2182–2189, 1965.

[86] E. B. Magrab and S. Azarm, *An engineer's guide to MATLAB.* Prentice Hall PTR, 2000.

[87] R. L. Panton, *Incompressible flow.* John Wiley & Sons, 2006.

[88] T. Johnson, "Conformal mapping in wing aerodynamics," 2013.

[89] E. L. Houghton and P. W. Carpenter, *Aerodynamics for engineering students.* Butterworth-Heinemann, 2003.

[90] J. C. Montgomery, C. F. Baker, and A. G. Carton, "The lateral line can mediate rheotaxis in fish," *Nature*, vol. 389, no. 6654, p. 960, 1997.

[91] J. D. Anderson, *Aircraft performance and design.* McGraw-Hill Science/Engineering/Math, 1999.

Curriculum Vitae

Fengying Dang is a PhD candidate in the Department of Electrical and Computer Engineering at George Mason University. She received the Bachelor's degree in Detection, Navigation and Control from Northwestern Polytechnic University, Xi'an, China, in 2015. Her research interests include bioinspired robotics, control systems, artificial intelligence, and underwater vehicles.